A Review of Advances in Dielectric and Electrical Conductivity Measurement in Soils Using Time Domain Reflectometry

D. A. Robinson,* S. B. Jones, J. M. Wraith, D. Or, and S. P. Friedman

ABSTRACT

Substantial advances in the measurement of water content and bulk soil electrical conductivity (EC) using time domain reflectometry (TDR) have been made in the last two decades. The key to TDR's success is its ability to accurately measure the permittivity of a material and the fact that there is a good relationship between the permittivity of a material and its water content. A further advantage is the ability to estimate water content and measure bulk soil EC simultaneously using TDR. The aim of this review is to summarize and examine advances that have been made in terms of measuring permittivity and bulk EC. The review examines issues such as the effective frequency of the TDR measurement and waveform analysis in dispersive dielectrics. The growing importance of both waveform simulation and inverse analysis of waveforms is highlighted. Such methods hold great potential for obtaining far more information from TDR waveform analysis. Probe design is considered in some detail and practical guidance is given for probe construction. The importance of TDR measurement sampling volume is considered and the relative energy storage density is modeled for a range of probe designs. Tables are provided that compare some of the different aspects of commercial TDR equipment, and the units are discussed in terms of their performance and their advantages and disadvantages. It is hoped that the review will provide an informative guide to the more technical aspects of permittivity and EC measurement using TDR for the novice and expert alike.

W ATER IS REQUIRED in some way by all living things; it is a fundamental constituent of life on our planet. Our survival as well as that of other organisms depends on a supply of water both to our own bodies and to the flora and fauna on which we live. One of the best ways to regulate water consumption is to know the quantity available and to manage the resource with prudence and stewardship (Hillel, 1991). To achieve this aim, techniques are preferred that can be used to measure a physical quantity closely related to the amount of water contained in a porous material, be it rock, soil, or an artificial medium.

The revolution in electronics in the latter half of the last century made the measurement of the electrical properties of materials more accessible than ever before. Measurement of the dielectric permittivity (dielectric constant) of a material emerged as an elegant method of estimating water content in porous materials. For the first time the same physical property (permittivity) could be measured for a range of scales and used to estimate water content. Electromagnetic methods, whether TDR (localized measurement), ground penetrating radar (two-dimensional profile), or active microwave remote sensing (land surface), all estimate water content based on the permittivity of the target medium. A further advance was the development of analysis methods using TDR. Time domain reflectometry was adapted to estimate both soil water content (Hoekstra and Delaney, 1974; Topp et al., 1980) and soil bulk EC simultaneously (Dalton et al., 1984). In spite of decades of research, we are only beginning to efficiently utilize electrical technology that ranges from satellite and airborne radar to ground penetrating radar and localized sensors such as TDR and impedance probes.

The underlying success of these techniques can be considered in two parts, the first of which is the equipment's ability to accurately measure the bulk dielectric permittivity and EC of a material. The second is the close relationship between the measured permittivity and the volumetric water content, or the ionic concentration and the bulk EC of the material. This review concentrates on the first stage, the accurate measurement of bulk permittivity and EC, and we confine ourselves to the use of TDR but acknowledge that other devices such as impedance probes (Dean et al., 1987; Hilhorst et al., 1993; Gaskin and Miller, 1996; Paltineanu and Starr, 1997) may also be used for this purpose. Time domain reflectometry has become a large topic in soil physics, primarily because of its adaptability and the continued development of novel applications. The focus of this review is on the measurement of bulk permittivity and EC, and thus some topics are dealt with only briefly or omitted. One of the strengths of the TDR measurement method is that many probes can be monitored almost simultaneously using a multiplexer (Baker and Allmaras, 1990; Heimovaara and Bouten, 1990; Herkelrath et al., 1991). This review discusses the measurement of bulk EC; however, we don't go any further to examine the interpretation of this in terms of soil solution conductivity. The literature on this aspect of TDR application is large, and the reader is referred to a recent publication for further reference (Dane and Topp, 2002). A further topic omitted from this review is the use of coated TDR probes. Coated probes have been proposed as a way to extend the working range of TDR in saline soils (Kelly et al., 1995; Nichol et al., 2002). However, the studies of Ferre et al. (1996) and Knight et al. (1997)

D.A. Robinson, U.S. Salinity Laboratory, USDA-ARS, 450 W. Big Springs Road, Riverside, CA 92507; S.B. Jones, Dep. Plants, Soils and Biometeorology, Utah State University, Logan, UT 84322-4820; J.M. Wraith, Land Resources & Environmental Sciences Dep., Montana State University, Bozeman, MT 59717-3120; D. Or, Dep. of Civil and Environmental Engineering, University of Connecticut, 261 Glenbrook Road, Unit 2037, Storrs, CT 06269; S.P. Friedman, Institute of Soil, Water and Environmental Sciences, The Volcani Center (ARO), Bet Dagan 50250, Israel. Received 21 Nov. 2002. Special Section—Advances in Measurement and Monitoring Methods. *Corresponding author (darobinson001@yahoo.co.uk).

Abbreviations: EC, electrical conductivity; TDR, time domain reflectometry.

indicate a strongly reduced sampling volume and questionable accuracy. Perhaps further investigation is needed to fully understand measurements made with such probes.

The history of using relative permittivity to estimate water content is confined to the last century, principally due to the measurement constraints imposed by the availability of instrumentation. It was recognized early on that the use of radio frequencies might be utilized to estimate water content. For example, Smith-Rose (1933, 1935) and Thomas (1966) gave accounts of early attempts to estimate moisture. However, not until the aftermath of the Second World War did the use of high-frequency electrical measurements in basic research really begin to expand. Dielectric theory had been well established, with Debye (1929) winning the Nobel Prize for his work on polar molecules. However, measurements had not kept pace with the advancing theory. The work of Hasted among others (Hasted et al., 1948; Ritson and Hasted, 1948; Hasted, 1973) stands out for pioneering work on the high-frequency measurement of permittivity, mostly in liquids. The pioneering work of Nelson et al. (1953) initiated a 50-yr contribution of research relating dielectric measurements to water content in vegetables, grains, and other composite porous media. Two distinct paths for permittivity measurement were seen to emerge in the 1960s. First, capacitance probes could be constructed following the development of small, high quality electrical components, (Thomas, 1966; Wobschall, 1978; Dean et al., 1987) and could be used for routine measurement in soils. Second, Fellner-Feldegg (1969) suggested the use of TDR for measuring permittivity, which was taken up in soil science by Hoekstra and Delaney (1974) and in the seminal work by Topp et al. (1980). Compared with capacitance probes, TDR's reduced susceptibility to signal interference, due to probe geometry and bulk EC as well as the minimal soil disturbance involved using multiple rods has led to its acceptance as a practical technique for measuring the permittivity of porous media (Cassel et al., 1994; Topp and Reynolds, 1998; Noborio, 2001; Dane and Topp, 2002). In the last 20 yr the earth sciences have successfully developed, applied, and expanded the use of TDR as a method for measuring permittivity and estimating water content, and it is now also being applied to measurements such as slope stability in geotechnical engineering (Dowding and O'Connor, 1999).

The Permittivity of Porous Media

Porous materials of interest in the earth sciences are usually composed of three components: the solid matrix, a gaseous phase, and the liquid water phase. The liquid water phase is sometimes subdivided further into free water and bound water, which is restricted in its mobility by adsorption on surfaces. The relative permittivity of air is 1, while those for common minerals in soils and rocks lie in the range 4.5 to 10 (Keller, 1989; Robinson and Friedman 2003), while water has a permittivity of 78.5 at 25°C. Thus the permittivity of any water bearing porous material is strongly influenced by its water content. The origin of the permittivity is the asymmetry of
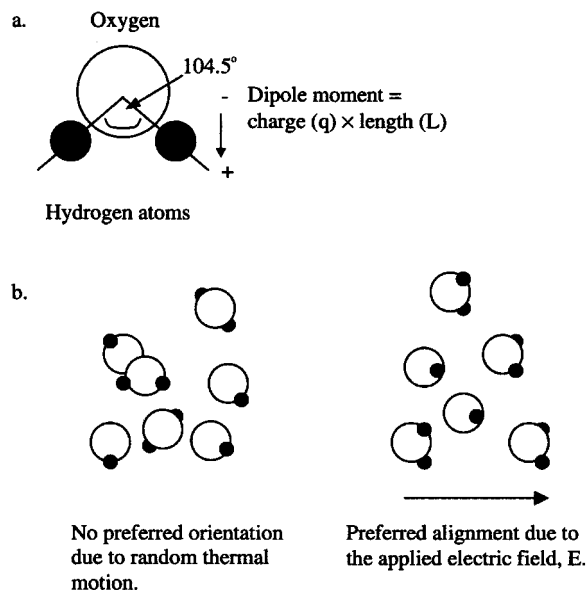
Fig. 1. (a) The dipole moment of a water molecule. (b) Water molecules randomly aligned (left) and being aligned by an external field (right). This alignment causes the storage of energy described as the real part of the permittivity.

charge in the water molecule (Fig. 1), which leads to a small displacement of the positive and negative charge centers creating a permanent dipole of 6.216×10^{-30} C m. When placed in an alternating electric field the molecules overcome their random thermal motion and align with the field (Fig. 1). The process of alignment stores electrical energy, which is released once the application of the field is stopped. This alignment of the molecules manifests itself as the real part of the relative permittivity (ε_r'). However, materials are rarely pure and usually contain some actual charge carriers such as ions. The loss of energy due to ionic conductivity is described by the imaginary part (ε_r''), termed *dielectric loss*. Another source of loss occurs when the molecules being aligned by the alternating field can no longer keep up with the speed of field alternation. The molecules are said to relax and energy is dissipated as heat. These properties are conveniently written as

$$\varepsilon_r = \frac{\varepsilon}{\varepsilon_o} \qquad [1]$$

Here the relative permittivity, ε_r is the ratio of the permittivity of the material, ε (F m^{-1}) to that of free space, ε_o (8.854 $\times$ 10^{-12} F m^{-1}). For a list of variables, see the Appendix.

$$\varepsilon_r^* = \varepsilon_r' - j\left(\varepsilon_{relax}'' + \frac{\sigma_{dc}}{2\pi f \varepsilon_o}\right) \qquad [2]$$

The complex relative permittivity ε_r^* describes energy storage and energy loss. The real part is designated ε_r' and associated with energy storage, and the imaginary components are associated with energy dissipation. Losses are associated with two main processes, molecular relaxation (ε_{relax}'') and electrical conductivity (σ_{dc}), where f is frequency and j is the imaginary number $\sqrt{-1}$.
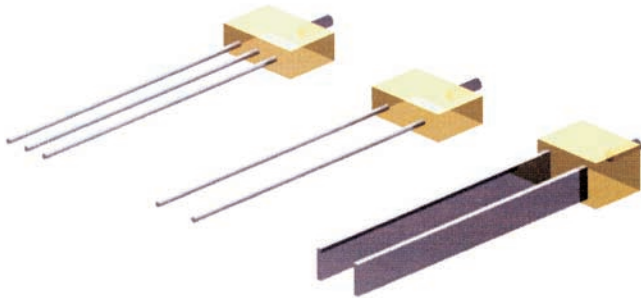
Fig. 2. Three TDR probe designs. Left to right, three-rod probe, two-rod probe, and parallel plate probe.

MEASUREMENT PRINCIPLES

Permittivity Measurement Using Travel Time Analysis along Transmission Lines

A transmission line forms the sensor for the TDR measuring system. Some classic designs are presented in Fig. 2. Their design and construction will determine the quality of the measurements made using the TDR technique; hence, we devote a major part of this review to designing and constructing probes to achieve optimal measurements. Transmission line theory is covered in detail in the literature (Kraus, 1984; Lorrain et al., 1988; Ibbotson, 1999), so in this section only an overview of the principles is given.

Time domain reflectometry measures the propagation velocity of a step voltage pulse with a bandwidth of around 20kHz to 1.5 GHz (Heimovaara, 1994). The velocity of this signal is primarily a function of the permittivity of the material through which it travels with potential modification by conductive losses. It is often convenient to consider the analogy of the propagation velocity of an electromagnetic plane wave that depends on the materials electromagnetic properties through which it travels:

$$v_p = \frac{1}{\sqrt{\mu_o \mu_r \varepsilon_o \varepsilon_r}} = \frac{c}{\sqrt{\mu_r \varepsilon_r}} \qquad [3]$$

where c is the velocity of light (3×10^8 m s^{-1}), ε_r is the relative permittivity, μ_o is the magnetic permeability of vacuum (1.257×10^{-6} H m^{-1}), and μ_r is the relative magnetic permeability. The relative magnetic permeability is unity in most earth materials, with the exception of some iron oxides (Robinson et al., 1994; Sharma, 1997).

Schematic diagrams of the TDR unit and a section of transmission line are presented in Fig. 3. A step voltage is applied between the conductors at the pulse generator. The signal propagates down the line and is reflected from the end of the probe; the returning signal is sampled in the TDR device. The velocity of the signal in a perfect dielectric is therefore

$$v = \frac{2l}{t}$$

and

$$v = \frac{c}{\sqrt{\varepsilon_r}} \qquad [4]$$

where l is the length (m) and t is the time (s) for a round trip (back and forth). Equating Eq. [4] and rearranging gives the round trip propagation time (t) of the wave as a function of both the length of transmission line (l) and the permittivity of the material:

$$t = \frac{2l \sqrt{\varepsilon_r}}{c} \qquad [5]$$

Hence it follows that the permittivity can be determined by measuring the time it takes the wave to traverse the probe. Waveforms for air and water are presented in Fig. 3 to demonstrate that the one-way travel time (e.g., the Tektronix [Beaverton, OR] cable tester divides the two-way travel time in half) is measured from the place marked "start" to the points marked "end reflection," and show that the travel time increases as the permittivity of the material increases.
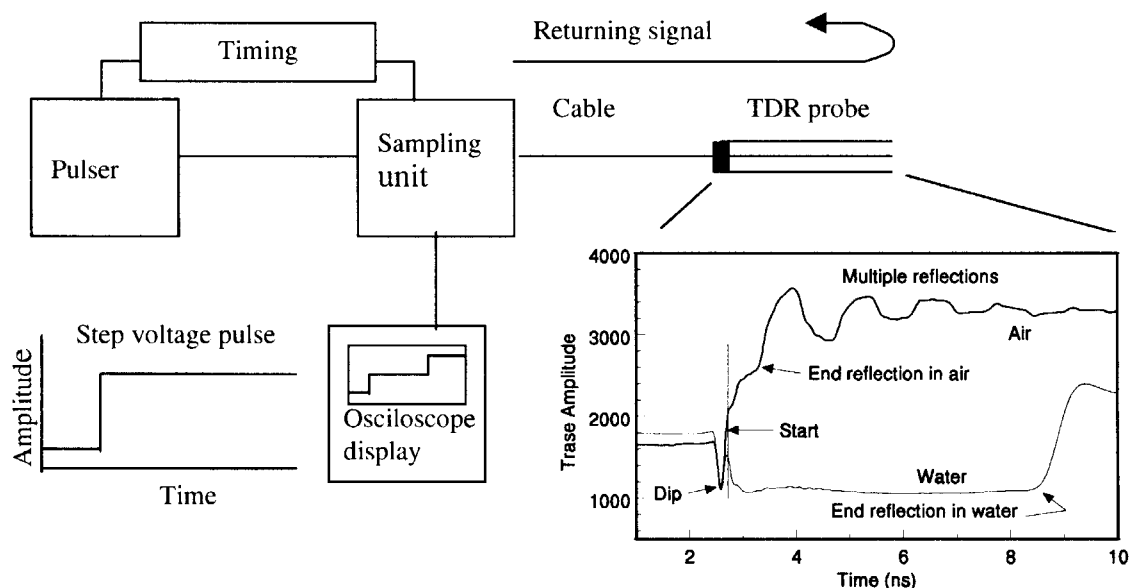

Fig. 3. A schematic diagram of the TDR main components. The window on the right illustrates two waveforms, one in air and one in water. The dip is caused by an electrical marker in the head of the TDR probe so that the software can locate the start point for travel time analysis.
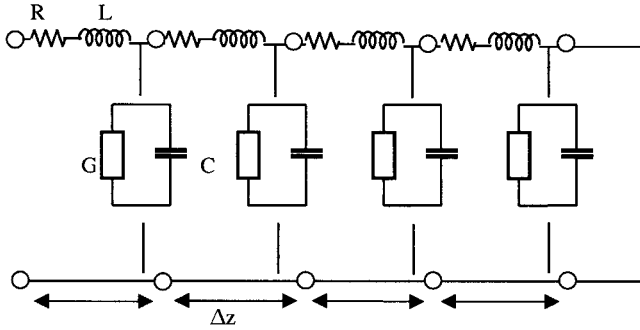
Fig. 4. Schematic diagram representing the electrical circuit analogy of a transmission line. L, R, C, and G are the line inductance, conductor skin resistance, medium capacitance, and medium conductance per unit length Δz.

Having determined how the overall system works it is helpful to examine how a plane wave propagates along a transmission line. A single-frequency, sinusoidal wave of angular frequency, ω (i.e., $2\pi f$), can be considered. A useful approach is to use the circuit diagram presented in Fig. 4. The transmission line can be analyzed as a circuit with series impedance (Z_s):

$$Z_s = R + j\omega L \qquad [6]$$

and a shunt admittance (Y), which is the inverse of the parallel impedances (Z_p):

$$Y = \frac{1}{Z_p} = G + j\omega C \qquad [7]$$

where L is the line inductance in series with a resistance R, which stems from the skin effect along the rod; C is the capacitance of the transmission line per unit length, dependent on material between and geometry of the TDR probe; and G is the transmission line conductance (Fig. 3). The line is then said to have a propagation constant, γ, which in general is a complex number, which is $\gamma = \sqrt{(Z_s Y)} = \alpha + j\beta$. The real ($\alpha$) and imaginary parts ($\beta$) are named the attenuation and phase constants respectively. From electromagnetic theory (Kraus, 1984)

the phase velocity v_p is determined from the phase constant β, the imaginary part of the propagation constant γ, according to

$$v_p = \frac{\omega}{\beta} = \frac{\omega}{\mathrm{Im}\sqrt{Z_s Y}} = \frac{\omega}{\mathrm{Im}\sqrt{(R + j\omega L)(G + j\omega C)}} \qquad [8]$$

In the case of a transmission line without losses Eq. [8] is often abbreviated to

$$v_p = \frac{\omega}{\omega\sqrt{LC}} = \frac{1}{\sqrt{LC}} \qquad [9]$$

It can be seen that if the wave is propagating along a real transmission line with a geometric factor g (m), a capacitance ($C = g\varepsilon_o\varepsilon_r$), and inductance [$L = (1/g)\mu_o\mu_r$], then the phase velocity in vacuum is the speed of light ($c = 3 \times 10^8$ m s^{-1}), and in any other material the equation for the velocity relative to that of light is according to Eq. [3]. In the case of a transmission line with some losses (where G is not $\ll \omega C$; Kraus, 1984) across the dielectric, the conductance term in Eq. [8] cannot be neglected and thus the velocity of the wave is modified. This reduces the velocity of the wave through the medium relative to that of light according to (Von Hippel, 1954)

$$v_p = \frac{1}{\sqrt{\dfrac{\mu_r\varepsilon_r'}{2}\left(1 + \sqrt{1 + \left\{\left[\varepsilon_{relax}'' + \left(\dfrac{\sigma_{dc}}{\omega\varepsilon_o}\right)\right]/\varepsilon_r'\right\}^2}\right)}} \qquad [10]$$

This means that the permittivity determined from the travel time analysis is no longer equivalent to the real part but to an apparent permittivity K_a (Topp et al., 1980; White et al., 1994). It is also a function of the dissipation across the rods caused either by relaxation losses (ε_{relax}'') or by electrical conductivity [$\sigma_{dc}/(\omega\varepsilon_o)$]. The effect of losses can be included into the equation for the measured apparent permittivity by combining Eq. [4] and [10] such that K_a is

$$K_a = \frac{\mu_r\varepsilon_r'}{2}\left(1 + \sqrt{1 + \left\{\left[\varepsilon_{relax}'' + \left(\frac{\sigma_{dc}}{\omega\varepsilon_o}\right)\right]/\varepsilon_r'\right\}^2}\right) \qquad [11]$$
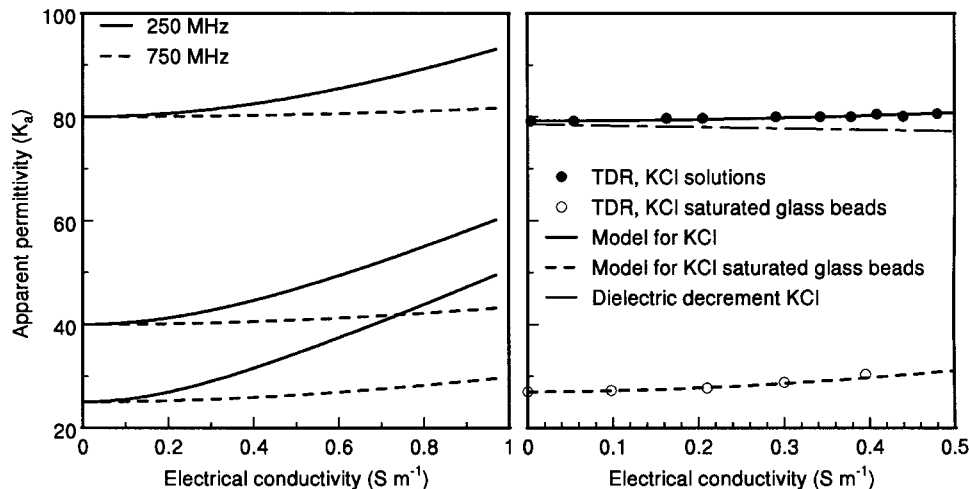

Fig. 5. Left, The apparent permittivity as a function of conductivity for two frequencies, 250 and 750 MHz. Permittivities of 80, 40, and 25 represent water, saturated clay, and saturated sand, respectively. Right, TDR measurements in KCl solutions and KCl saturated glass beads, Eq. [11] fitted using a frequency of 400 MHz as the effective frequency.
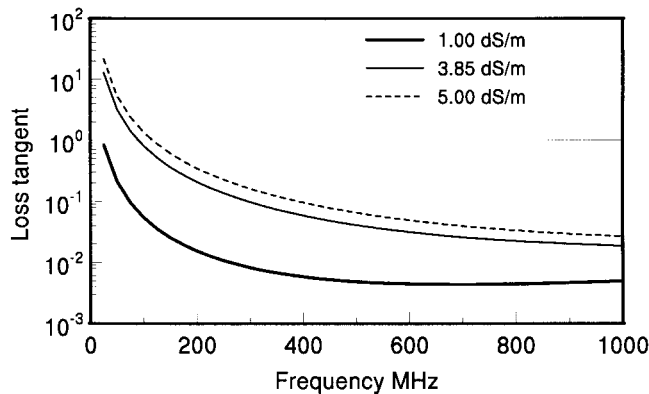
Fig. 6. The loss tangent (tan²δ) as a function of frequency for three differing bulk electrical conductivities.

As the losses become more significant the propagation time increases, and thus higher apparent permittivity values are measured (Fig. 5). The difficulty in applying an equation such as Eq. [11] is that it is formulated for a plane wave at a single frequency; TDR is a broadband technique and a waveform is composed of many frequencies. However, the data presented in Fig. 5 tend to confirm that the general impact of low ionic conductivity (~10 dS m^{-1}) values can be described by Eq. [11]. In the case of the two independent data sets presented, one for KCl solution and the other for KCl saturated glass beads, 400 MHz was found to be an appropriate effective frequency. This effective frequency is unlikely to be universal. It will depend on the TDR device used, the construction of the probe, and the dispersive nature of the dielectric.

The loss tangent (tan²δ) refers to the ratio of the imaginary to real permittivity.

$$\tan^2\delta = \left\{ \left[\varepsilon''_{\text{relax}} + \left(\frac{\sigma_{\text{dc}}}{2\pi f \varepsilon_o} \right) \right] \Big/ \varepsilon'_r \right\}^2 \qquad [12]$$

One aim of designing probes used solely for measuring water content is to minimize electrical conductance across the probe. This is achieved by having rods with a low geometric factor, g, (reciprocal of the commonly used cell constant, m^{-1}), which is discussed below in the section on probe design. Assuming that the imaginary permittivity and conductivity terms are small means K_a and ε'_r can be considered equivalent. An important aspect of the measurement that impacts both the real and imaginary permittivity is what might be termed an *effective frequency* (f in Eq. [12]). This is important because according to Eq. [12] the magnitude of the loss tangent due to EC will depend on this effective frequency. Figure 6 illustrates loss tangents for several electrical conductivities and clearly demonstrates how they increase in the lower frequencies, resulting in increasing imaginary permittivity.

INTERPRETING AND MODELING WAVEFORMS

Dispersive Media and Effective TDR Frequency

Waveform interpretation can be best understood when an understanding of what is being measured is clear. The TDR waveform reflects the electrical properties of the material through which it travels and is determined
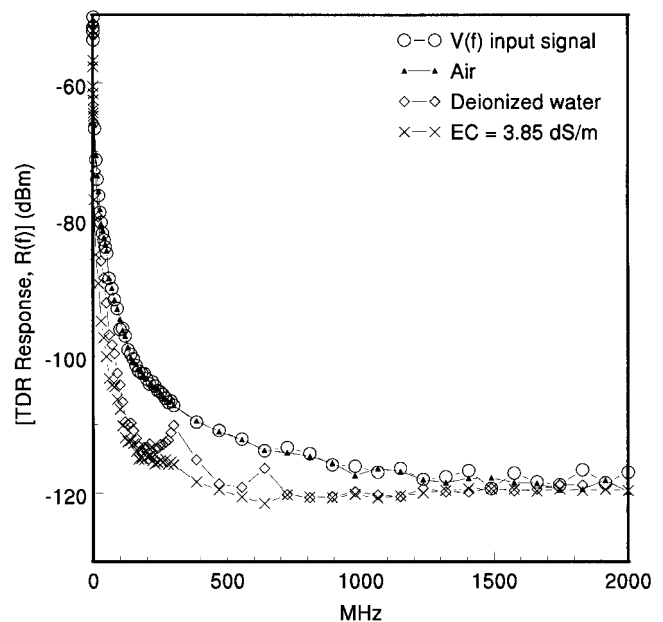

Fig. 7. Spectrum analyzer measurements for air, water, and a saline solution (data from Friel and Or, 1999). The TDR was connected through a coaxial cell to a spectrum analyzer. The results give the TDR power response as a function of frequency.

by the amount of power at each frequency measured that combine to make the waveform. Friel and Or (1999) took a direct series of measurements of TDR power output with a sample connected from the TDR to a spectrum analyzer, showing an inverse square decrease in power as a function of frequency ($\propto 1/f^2$) in air. Results for air, water, and an electrolyte solution are presented in Fig. 7 and show that most of the power is below 500 MHz. This graph is useful in demonstrating how a dielectric with a high permittivity like water (80) reduces the power at all frequencies but especially the higher ones. The results are presented up to 2GHz; above 1.5 GHz the signal is mostly noise (i.e., lower than −120 dBm). The introduction of a salt into the water further reduces the power at each frequency. This graph provides useful insight when we discuss the issue of effective frequency raised at the end of this section. An effective frequency can be defined in several ways, and we shall examine each of these and its implications.

Or and Rasmussen (1999) defined the effective frequency as the highest frequency component of the signal passing through the dielectric without being filtered. Using tangent lines fitted to the TDR waveform, they measured the permittivity of ethanol–water mixtures and then compared them with the real permittivity measured as a function of frequency using a network analyzer. They fitted a curve to give the effective frequency (f^*) as a function of the TDR measured permittivity:

$$f^* = f_\infty (1 - e^{-\alpha\varepsilon}) \qquad [13]$$

where $f_\infty = 2.34$ GHz and $\alpha = 0.0216$. They suggested frequencies ranging between about 550 MHz at low permittivity values and high dispersion and 1.8 GHz at the permittivity of water (80) with low dispersion. To understand this a little better we examine each of these steps in the time and frequency domains for a dispersive dielectric.
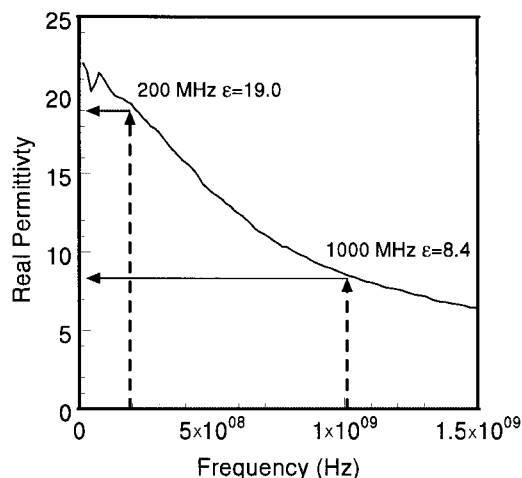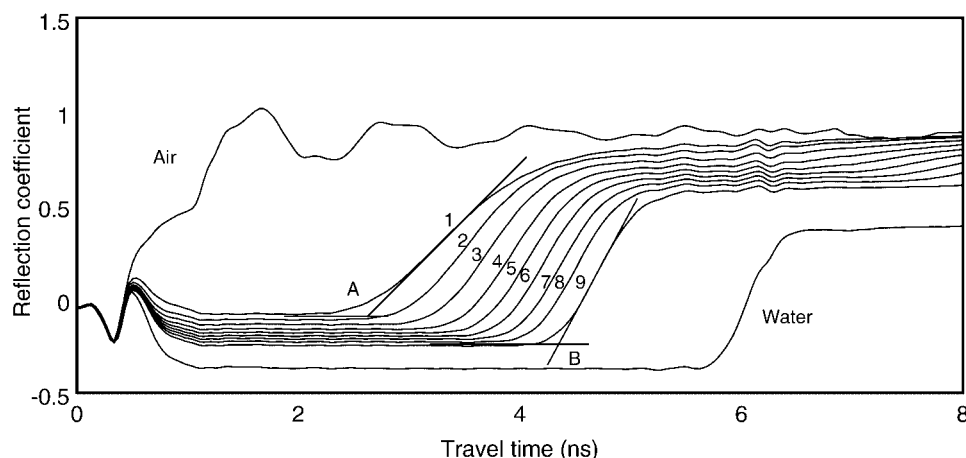
Fig. 8. The real permittivity of propanol with some absorbed water. The arrows demonstrate that a 200-MHz signal will "see" a permittivity of 19.0, whereas a signal with a frequency of 1000 MHz will "see" a permittivity of 8.4. The high-frequency signal will therefore travel faster than the low-frequency signal which sees a higher permittivity.

Careful TDR calibration can result in accurate (± 0.1) measurement of permittivity. However, many materials, especially soils, can be dispersive, which makes waveform interpretation and permittivity measurement more difficult (Heimovaara, 2001). A dielectric material is dispersive if it suffers from relaxation in the measurement bandwidth (0.001–1.75 GHz). For example, air is nondispersive and water is effectively nondispersive, as its relaxation frequency (17 GHz) is well outside the TDR's frequency bandwidth. However, most alcohols and many soils exhibit relaxations under 1 GHz. The cause of this relaxation in soils can be due to the reduced mobility of water near surfaces Maxwell Wagner relaxation, and it is especially pronounced in the high surface area clay soils. When such a material demonstrates relaxation within the TDR measurement bandwidth, it causes dispersion. The input signal of the TDR is composed of many frequencies, and at the start these are all in phase. In a dispersive medium, the different frequency components of the input signal travel at different speeds. This is caused by the real permittivity changing

as a function of frequency and is presented diagrammatically in Fig. 8 using a measurement made in propanol as an example. The arrows indicate that a frequency of 200 MHz will effectively "see" a permittivity of 19.0, while a frequency of 1 GHz will "see" a permittivity of 8.4. Since waves travel faster in materials with low permittivity, the signal no longer travels in phase but spreads out. This can be observed by examining the TDR waveforms in Fig. 9. The waveforms are for mixtures of propanol and water, Waveform 1 is propanol with a little absorbed water, and the proportion of water increases from waveform 2 to 9. The slope of the second reflection increases as more water is added to the propanol; the waveform becomes sharper and more distinct. Figure 10 shows the corresponding real part of the permittivity in the frequency domain for the 9 propanol–water mixtures corresponding to the waveforms in Fig. 9. The arrows indicate the method of Or and Rasmussen (1999) using the measured TDR permittivity by fitting tangent lines (A in Fig. 9) and using this to obtain a frequency f^* corresponding to the highest frequency component in the measurement. From inverse analysis of waveforms (Heimovaara, 2001; Weerts et al., 2001) we know that the point at which the tangent lines intersect for a waveform represents the fastest moving part of the signal. We can therefore see that this frequency, f^*, changes a lot as dispersion increases.

The issue of the importance of an effective frequency was raised by Topp et al. (2000) as it is required if Eq. [11] is to be used to try and obtain a real permittivity from the apparent permittivity (K_a) measured by the TDR. In the case of this effective frequency it is likely that it should reflect the frequency where the majority of the energy of the signal is contained. Thus, an alternative determination of an effective frequency was proposed by Topp et al. (2000). They suggested using what they termed the *maximum passable frequency* for the sensor, which they denoted f_{max}. They suggested that an estimate of this value can be obtained from the rise time of the reflection from the end of the TDR probe after it has traveled through a dielectric material. This method has been utilized by previous workers (Hilhorst, 1998; Sun et al., 2000), and an outline of the method is given in

Fig. 9. Waveforms collected with a 0.18-m coaxial cell for air, water, and propanol–water mixtures. Waveforms 1 through 9 have increasing amounts of water. Location A shows how tangent lines were fitted to the waveforms.
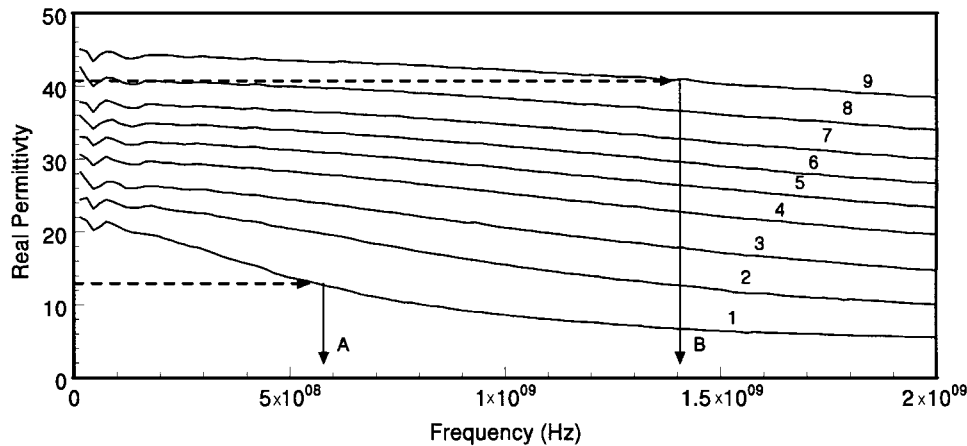
Fig. 10. The real permittivity of the propanol–water mixtures corresponding to Fig. 9. The arrows indicate the permittivity values measured from the waveforms in Fig. 9 used to determine the frequency to which they correspond.

Appendix C of the Tektronix application note entitled, "TDR's for Cable Testing." The rise time is measured as the time between 10 and 90% of the signal magnitude illustrated in Fig. 11. An example of the analysis required to determine the rise time value (t_r) is presented in this figure. The value of f_{max} is then calculated according to (Strickland, 1970)

$$f_{max} = \frac{\ln(0.9/0.1)}{2\pi t_r} \qquad [14]$$

this simplifies to f_{max} (Hz) = 0.35/t_r, where t_r is measured in seconds. The above method was used by Topp et al. (2000) to estimate the effective frequency for TDR measurements made in soils with clays; they suggested frequency bandwidths between 100 and 400 MHz.

In Fig. 12 we compare results using the two methods for the propanol–water mixtures presented in Fig. 9. The value obtained for the frequency using Eq. [14] is consistently about 0.45 of the value obtained using the Or and Rasmussen (1999) method. This frequency value probably reflects a location where most of the energy of the signal is located. It would be interesting to see in future work if this determined value corresponds with

the location of the group velocity of the signal, which is the speed of the wave packet. The terminology used by Topp et al. (2000) of the maximum passable frequency is perhaps misleading and should be dispensed with in light of the comparison with the method of Or and Rasmussen (1999). With regard to terminology, the frequency obtained by Or and Rasmussen (1999) should be considered the *maximum frequency*, f^*, and that obtained from Eq. [14] perhaps an *effective frequency*, f_{eff}. Interestingly, in nondispersive media both methods give similar values for the highest frequency. The line at the top of the graph indicates the frequency (1.8 GHz) obtained in water using the Or and Rasmussen (1999) method. This is in close agreement with the value of 1.75 GHz given by the Tektronix application note entitled, "TDR's for Cable Testing." The diagram also indicates that the frequency determined by either method will reduce if the material is dispersive in the TDR bandwidth (arrows and dashed line). The curve presented by Or and Rasmussen (1999) indicates values of f^* to be expected with water–alcohol mixtures. However, this

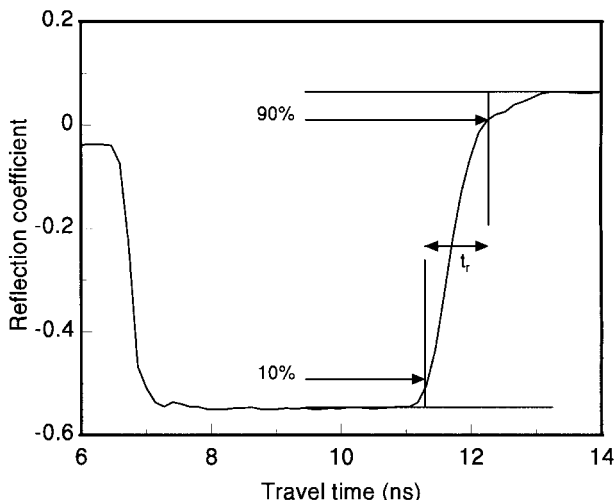Fig. 11. Demonstration of the method used to estimate the highest passable frequency for a given material. t_r is the time measured between the signal rising 10 to 90% of the signal magnitude.
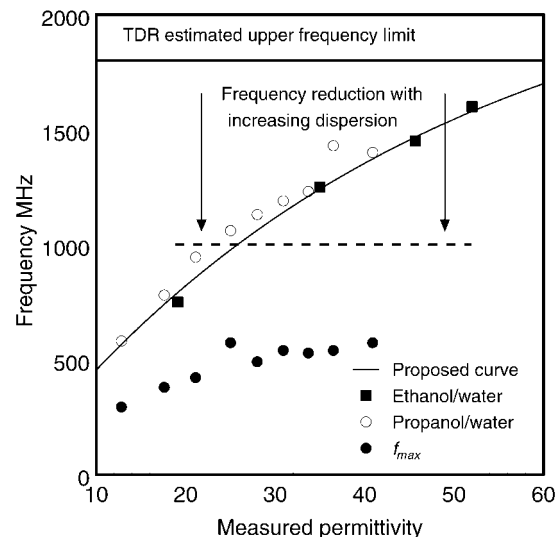

Fig. 12. The effective frequencies determined from Fig. 10 and the data of Or and Rasmussen (1999). The filled circles represent the corresponding effective frequency (f_{max}) calculated using Eq. [14].
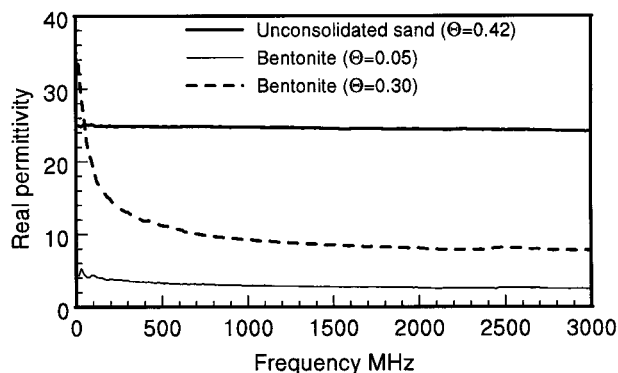
Fig. 13. The real permittivity measured for saturated quartz sand and bentonite clay at two water contents. The figure demonstrates the sharply changing real permittivity of moist bentonite below 500 MHz.
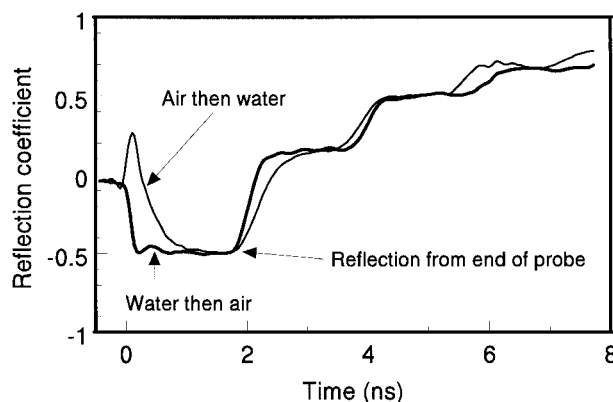

Fig. 14. Waveforms from layered water and air with the respective order changed. The shape of the waveforms changes but the travel time remains the same.

is likely to vary depending on the permittivity of the material and its relaxation time.

This has interesting implications for measurements made in heavy clay and mineral soils. Figure 13 presents dielectric spectra of water-saturated quartz sand and bentonite clay at two water contents, 0.05 and 0.30 m³ m⁻³. These spectra indicate that for a granular material like saturated quartz grains the real permittivity doesn't change much in the TDR frequency bandwidth. However, the real part of the permittivity for the bentonite changes dramatically below 500 MHz. Behavior like this will undoubtedly affect TDR waveforms and permittivity measurements. In the TDR soil literature, measurements made on bentonite (Dirksen and Dasberg, 1993) showed a sharp rise in the apparent permittivity at water contents above 0.25 m³ m⁻³. The permittivity values measured rose above the calibration of Topp et al. (1980). This behavior is in agreement with the description of measurement in dispersive media. For the case of dispersive clayey soils we can expect the reverse behavior of the propanol–water mixtures presented in Fig. 12. The increasing real permittivity observed for bentonite in Fig. 13 was also observed to increase as the water content increased (data not shown). Thus, at higher water contents more dispersion occurs, with which we would expect lower frequencies (<500 MHz). With lower frequencies at higher water contents, we'd expect to see an increase in permittivity, which is what has been observed in the data of Dirksen and Dasberg (1993) for bentonite. An important point to make is that not all clay soils will be dispersive. It is likely that the soils used in Topp's original work (Topp et al., 1980) were nondispersive, hence their optimistic suggestion of a universal calibration for soils.

These findings raise the issue of what is an appropriate permittivity measurement in a dispersive soil. Measurement frequency in dispersive soils will change as a function of water content, as will the real part of the permittivity. The use of permittivity determined by travel time analysis may not be the most appropriate value. It is preferable to have a value for a fixed frequency, preferably above the frequencies where relaxation strongly affects the real part of the permittivity. Some workers have suggested the use of alternative methods of interpreting waveforms for dispersive media. Huisman et al.

(2002) suggested fitting a simulated waveform with frequency-dependent parameters to the captured waveform. By doing this, a frequency could be chosen at which to determine the permittivity from the best-fitted relaxation equation, $\varepsilon^*(f)$. They tested this method in a sandy soil, which unfortunately had insufficient relaxation to test this idea thoroughly. Lin (2003b) used both Debye and volumetric mixing models to describe the frequency-dependent characteristics of the soil so that simulated waveforms could be fitted to the measured waveforms. He concluded that both methods appeared to give a reasonable description of the frequency response of the soils. This approach opens a new way to interpreting TDR information and along with inverse analysis of waveforms could lead to more comprehensive understanding of the soil permittivity–water content relationship.

Interpretation of Waveforms in Layered Media

An important phenomenon encountered in many natural porous media such as soils and sediments is the presence of sharp wetting and drying fronts of contrasting zones of wet and dry layers, which have corresponding contrasting permittivity values. Because TDR rods are often placed vertically downward, these layers are likely to be bisected. The impact this has on the waveform is presented in Fig. 14. Both waveforms were obtained with 50% water and 50% air; however, one has water over air and the other air over water. What is apparent from these waveforms is that they have different shapes depending on whether air (low permittivity) or water (high permittivity) comes first, but the travel time is still the same.

The issue of TDR measurements across a wetting or drying front was examined in a number of articles (Topp et al., 1982a; Nadler et al., 1991; Dasberg and Hopmans, 1992; Feng et al., 1999; Timlin and Pachepsky, 2002). Topp et al. (1982a) produced a two-layer model based on summing the travel times of the TDR signal in the layers.
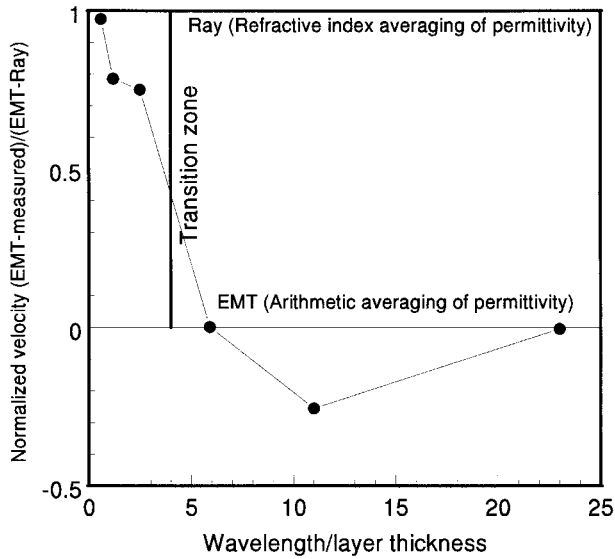
$$t_{tot} = t_1 + t_2$$

[15]

Fig. 15. Measurements from Chan and Knight (2001) for the change in velocity averaging. As the wavelength/layer thickness ratio increases above 4, the permittivity averaging changes from refractive index to arithmetic.

$$\sqrt{K_a} = \frac{ct_{tot}}{L_{tot}} = \frac{L_1\sqrt{K_1} + L_2\sqrt{K_2}}{L_{tot}} \quad [16]$$

A similar experiment considering the two soil layers as two separate sections of a transmission line allowed Feng et al. (1999) to model the TDR waveforms of layered systems with realistic results.

Chan and Knight (1999, 2001) demonstrated that averaging of the propagation velocity through a layered media changes depending on the ratio wavelength/layer thickness (Fig. 15). In terms of permittivity, the averaging changes from refractive index averaging, which they term *ray theory*, to arithmetic averaging, termed *effective medium theory*, with the transition zone occurring at a wavelength to layer thickness ratio of about 4. This value corresponds to the layers being one-quarter wavelength thick. When the layers are becoming thin, and effectively invisible to the traveling wave, the situation is similar to that of making the K_a the arithmetic mean of the fractions of solid and water. This is analogous to the case when the electric field is parallel to the layering of an anisotropic medium made of infinitely thin disk-shaped particles (Jones and Friedman, 2000)

$$\sqrt{K_a} = \frac{L_1\sqrt{K_1} + L_2\sqrt{K_2}}{L_{tot}} \xrightarrow{\frac{\lambda}{L} \geq 4} K_a = \frac{L_1 K_1 + L_2 K_1}{L_{tot}} \quad [17]$$

Chan and Knight (2001) demonstrated this with TDR measurements in layers of dry coarse sand and fine wet sand, presented in terms of normalized velocity ($v_{normalized}$) in Fig. 15:

$$v_{normalized} = \frac{v_{EMT} - v_{measured}}{v_{EMT} - v_{ray}} \quad [18]$$

In the figure the wavelength divided by layer thickness is presented. However, in light of the discussion about effective frequency and the difficulty of assigning an effective frequency or wavelength to TDR measurements,
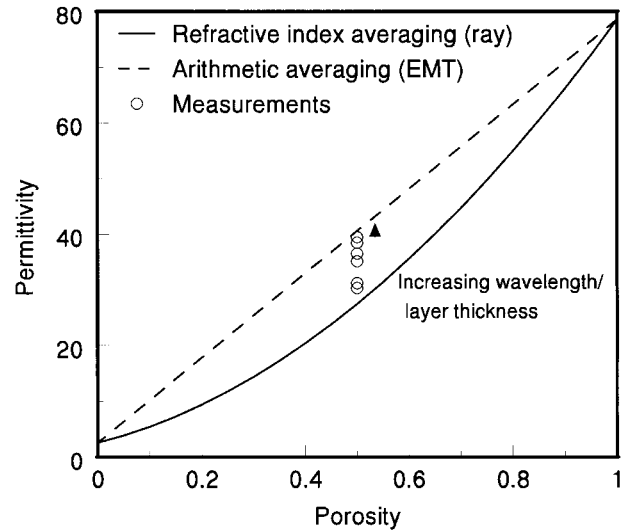

Fig. 16. Refractive index and arithmetic averaging of permittivity for layers of Plexiglas and water. As the wavelength/layer thickness ratio increases above 4, the averaging moves from refractive index to arithmetic, as indicated by the arrow (Schaap et al., 2003).

Schaap et al. (2003) proposed that it was more appropriate to plot the normalized velocity as a function of layer thickness. Measurements made with alternating disks of water (78.5) and Plexiglas (3.5) are presented in Fig. 16. They demonstrate the two averaging regimes for TDR measurements in layered media, refractive index (Eq. [19]) and arithmetic (Eq. [20]). The arrow points in the direction of increasing wavelength/thickness ratio.

$$\sqrt{K_a} = \left(\frac{\theta}{\theta_s}\right)\sqrt{K_{water}} + \left(1 - \frac{\theta}{\theta_s}\right)\sqrt{K_{Plexiglas}} \quad [19]$$

$$K_a = \left(\frac{\theta}{\theta_s}\right)K_{water} + \left(1 - \frac{\theta}{\theta_s}\right)K_{Plexiglas} \quad [20]$$

In these equations, θ is the fractional water length (volumetric water content) and K_{water} and $K_{Plexiglas}$ denote the permittivity of the water and Plexiglas, respectively.

The potential of waveform simulation was suggested in the above discussion concerning dispersive media. Again it offers great potential for understanding the response in layered materials (Feng et al., 1999). Timlin and Pachepsky (2002) showed how fitting simulated waveforms to the measured waveforms with vertical probes could be used to obtain infiltration rates for the soil. Simulated and measured waveforms from Schaap et al. (2003) for the data shown in Fig. 16 are presented in Fig. 17. In the simulated waveforms the probe head was omitted from the modeling, as it was unnecessary for the qualitative comparison. Information obtained from this approach allowed Schaap et al. (2003) to demonstrate the frequency dependence of the permittivity averaging of the layering in their paper. They observed that at the lower frequencies (<100 MHz) all layers studied needed to be averaged using the arithmetic averaging. At higher frequencies thin layers remained in the arithmetic-averaging regime, while thicker layers were averaged according to the refractive index averaging regime. The refractive index averaging regime will be appropriate for most soils and TDR probe lengths. An
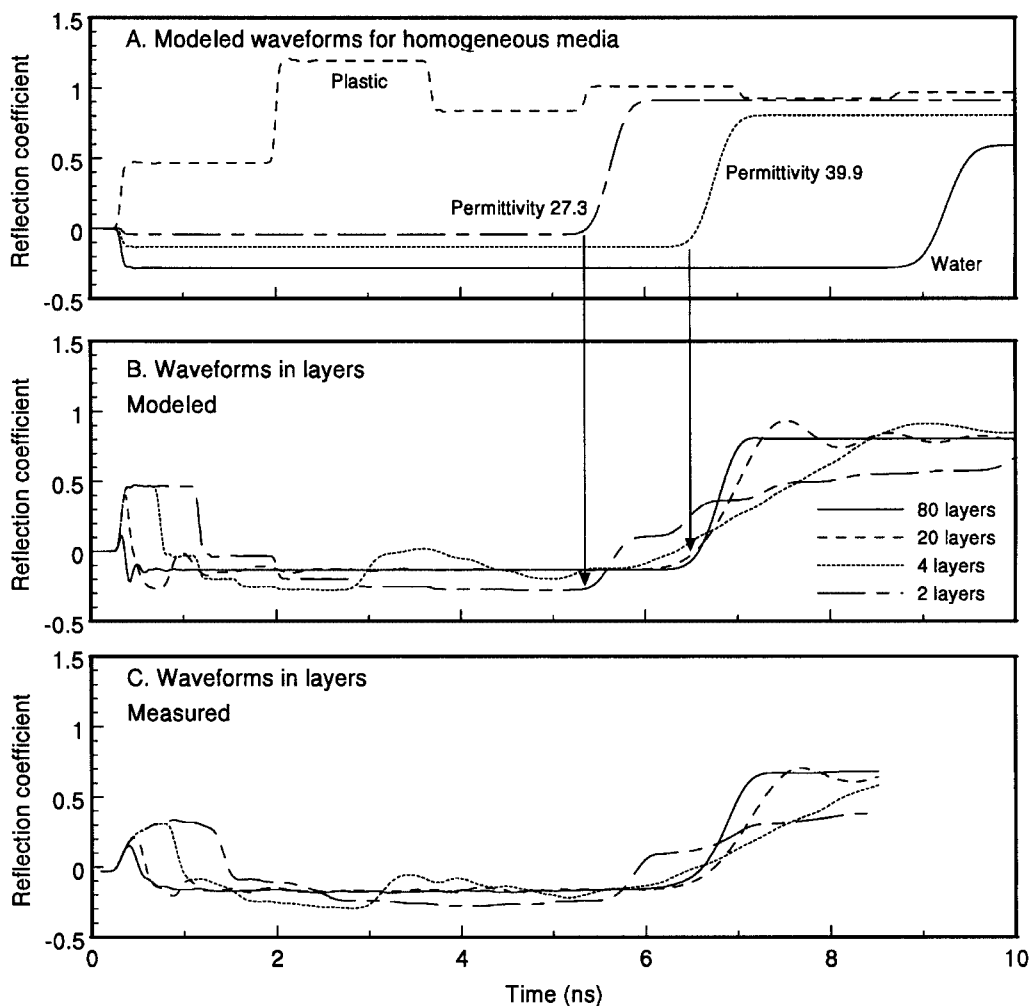
Fig. 17. Modeled and measured waveforms for layers of Plexiglas and water. (A) Modeled waveforms for homogeneous dielectric. (B) Modeled waveforms for layered dielectrics. (C) Measured waveforms for layered dielectrics corresponding to those modeled in Fig. 17B. (From Schaap et al., 2003).

experiment using coarse sand was used to test this. Seven hundred–micrometer quartz sand was wetted from the base of a 0.18-m-tall cell with a 0.15-m-long parallel plate probe in it. The data presented in Fig. 18, measured with the TDR, confirm that refractive index averaging is appropriate.

TDR Waveform Theory and Modeling

The above discussion indicates the potential of both simulating waveforms and conducting inverse analysis on waveforms to obtain greater information content. Transitioning between time and frequency domains is of interest for extending the information content extracted from TDR measurements. Waveforms obtained for travel time analyses rely on proper identification of markers for accurate permittivity determination and subsequent water content estimation. Early efforts to streamline this process were aimed at automating waveform analysis techniques (Baker and Allmaras, 1990; Heimovaara and Bouten, 1990). In recent years, advanced means of analyzing waveforms have been developed that extend the information content beyond conventional travel-time
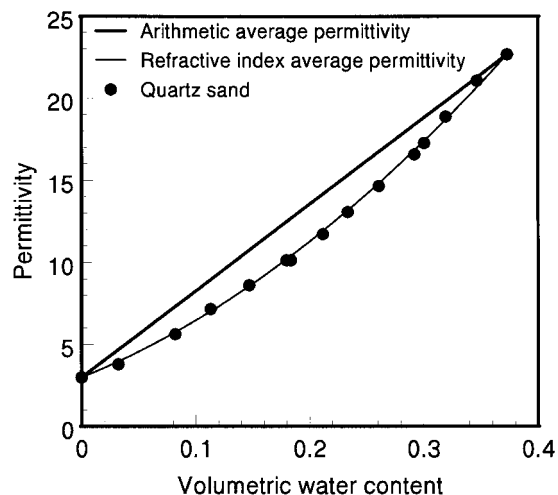

Fig. 18. Measurements of the permittivity of coarse grained (700 μm) monosized quartz sand. The data and modeling suggest that for these measurements the averaging remains in the refractive index regime.

analysis illustrated in Fig. 30. Information on the complex dielectric permittivity is embedded within the waveform captured in the time domain and may be extracted in the frequency domain using Fourier analysis. Inverse Fourier analysis may be used to fit frequency-dependent model parameters to waveforms in the time domain. In the time domain, the input signal, $v_o(t)$, describes the cable tester, cable, and probe head, and the response function, $r(t)$, describes the entire system, including the sample being measured. These are obtained from TDR waveforms measured in air and in the sample material. The measurement in air may have the central conductor pin removed from the coaxial sample holder, or the input function may be modeled. The system response, $s(t)$, contains information on the sample's dielectric permittivity, where $r(t)$ is described by the following convolution integral (van Gemert, 1973):

$$r(t) = \int_{-\infty}^{t} v_0(t - \tau)s(t)\mathrm{d}\tau \qquad [21]$$

where τ is the variable of integration and $s(t)$ describes how an input signal will be modified by the sample. The discrete fast Fourier transform of both $v_o(t)$ and $r(t)$ reduce the unsolvable convolution theorem integral to a simple algebraic expression describing the scatter or system function, $S_{11}(f)$, in terms of the frequency-dependent response, $R(f)$, and input, $V_0(f)$, functions, given by Lathi (1992) as

$$S_{11}(f) = \frac{R(f)}{V_o(f)} \qquad [22]$$

Alternative transmission line modeling approaches have been demonstrated which describe the waveform using a wave propagation model, accounting for multiple reflections of the segmented system (e.g., cable, head, and probe), and described in terms of input impedance (Lin, 2003a, 2003b; Feng et al., 1999). The determination of sample properties is (i.e., ε, σ_{dc}, f_{rel}) generally performed by fitting model parameters to the discrete measured waveform. This fitting may take place in the time domain, or after Fourier transform, the fitting may take place in the frequency domain. The theoretical basis of many of these approaches relies on a coaxial probe geometry, which is only approximated by multirod probe designs. Data presented in both domains are illustrated in Fig. 19, where the discrete data from the waveform, V_i, measured in the time domain are presented in Fig. 19a. The reflection coefficient is determined from the measured waveform voltages, described as

$$\rho = \frac{V_i - V_o}{V_o - V_{ref}} \qquad [23]$$

where V_o is the voltage in the cable before entering the probe and V_{ref} is the voltage in the cable tester (i.e., at -0.6 m in the Tektronix 1502), sometimes assumed to be zero. These were transformed to frequency-dependent discrete data points making up the scatter function shown in Fig. 19b. Waveform transformation procedures and
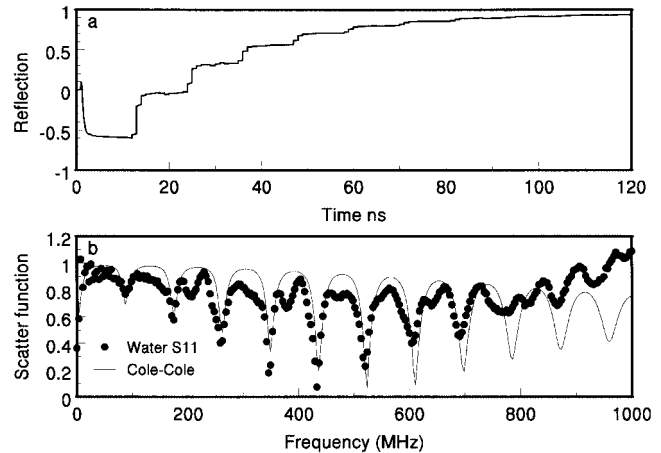

Fig. 19. (a) TDR waveform in water. (b) The corresponding scatter function for water measured using TDR and modeled using the Cole–Cole (1941) relation.

results are described by a number of authors (Heimovaara, 1994; Friel and Or, 1999; Weerts et al., 2001).

Time Domain Analysis

A multisection approach may be used to reconstruct waveforms in the time domain (Yanuka et al., 1988; Feng et al., 1999; Heimovaara, 2001; Robinson et al., 2003; Schaap et al., 2003). Variations of this approach attempt to describe the cable–head–sample system using a multisection scatter function, which may again be linked to the complex dielectric permittivity of the soil. Feng et al. (1999) demonstrated the usefulness of this multisection approach for extracting information from multilayered soils oriented perpendicular to the propagating electrical signal. Heimovaara (2001) demonstrated the potential for extracting information on signal dispersion and subsequently on the soil properties from inverse analysis. Greater information content is possible using optimization techniques coupled with dielectric mixing model parameters describing the frequency-dependent character of soil constituents (Heimovaara et al., 1996; Friel and Or, 1999; Lin, 2003a). Using inverse analysis of 2000 simulated TDR waveforms, Weerts et al. (2001) examined Debye model parameter sensitivity and determined correlations between model parameters and waveform characteristics. They found bulk EC to have the strongest influence on the waveform character. Both high-frequency and static permittivity parameters had a significant influence in waveform modeling, but each were capable of fitting waveforms under three possible scenarios dependent on the relaxation frequency selection. The three scenarios show the dispersion curve within the TDR frequency bandwidth being (i) cut off by the low frequency limit, (ii) cut off by the high frequency limit, or (iii) completely contained within the frequency bandwidth of the waveform data. Further refinement of these techniques should improve the information content and reliability of analysis for studying relaxation phenomena and complex permittivity determination.

Frequency Domain Analysis

The frequency content of the measured TDR waveform extends from about 20 kHz to roughly 1.5 GHz

(Heimovaara, 1994; Fig. 7). The quality of the measurement equipment, the permittivity of the dielectric and its lossy nature, as well as probe geometry, may influence this range. Frequency-dependent information may be determined by fitting an appropriate model to the transformed scatter function in the frequency domain. One such model describes the multiple reflections of an open-ended coaxial transmission line, which can be modeled according to the scatter function given by Clarkson et al. (1977) as

$$S_{11}(f) = \frac{\rho + e^{-2\gamma L}}{1 + \rho e^{-2\gamma L}} \qquad [24]$$

in which L (m) is the probe length and where ρ is the reflection coefficient described as

$$\rho = \frac{1 - z\sqrt{\varepsilon_r^*(f)}}{1 + z\sqrt{\varepsilon_r^*(f)}} \qquad [25]$$

in which $z = z_c/z_p$ is the impedance ratio of the cable, z_c, and probe, z_p, and where γ is the transverse electromagnetic mode propagation constant written as

$$\gamma = \frac{j2\pi f\sqrt{\varepsilon_r^*(f)}}{c} \qquad [26]$$

Heimovaara (1994) and Friel and Or (1999) adopted a modified form of the Debye (1929) model by Cole and Cole (1941) to fit $\varepsilon^*(f)$ to scatter function data, using parameters describing the static and high-frequency dielectric permittivity, relaxation frequency, and EC of different liquids:

$$\varepsilon_r^*(f) = \varepsilon_\infty + \left\{ \frac{\varepsilon_{s,cc} - \varepsilon_\infty}{1 + [j(f/f_{rel})]^{1-\beta_{cc}}} \right\} - \frac{j\sigma_{dc}}{2\pi f\varepsilon_o} \qquad [27]$$

where, ε_∞ is the high-frequency limit of the real permittivity, $\varepsilon_{s,cc}$ is the static value of the real permittivity, f is the measurement frequency (Hz), f_{rel} is the mean relaxation frequency, β_{cc} is a parameter accounting for a spread in relaxation frequency, σ_{dc} is the solution electrical conductivity (S m^{-1}), and j is the imaginary number $\sqrt{-1}$. Lin (2003b) built on this approach and modeled the frequency-dependent dielectric permittivity of soil constituents (i.e., solid, air, water, and bound water) using the Debye (1929) model. These dielectric components were incorporated into the dielectric mixing model of Dobson et al. (1985) and fitted in the frequency domain. Information lost due to attenuation under lossy conditions is less detrimental for a frequency domain analysis than the second reflection determination in a time domain analysis. Jones and Or (2001) coupled frequency domain analysis with the use of short (0.02–0.06 m) TDR probes to extend the TDR measurement range in saline soils. Permittivity determination was increased to bulk EC levels eight times greater than realized using conventional time domain analysis with a 0.15-m probe.

Electrical Conductivity Measurement Using TDR

One of the great strengths of TDR is that it can be used to measure bulk EC in addition to permittivity (Dalton et al., 1984; Topp et al., 1988; Dalton, 1992; Nadler et al., 1991; Heimovaara and de Water, 1993; Mojid et al., 1997). This section examines the principal way of measuring the EC from TDR waveforms and an alternative broadband conductivity method.

The Method of Giese and Tiemann

Giese and Tiemann (1975) are credited with the first determination of sample resistance using TDR waveforms. This is equivalent to measuring the low-frequency resistance across the sample between the probe rods and has been used by Nadler et al. (1991). Heimovaara (1993) also used the reflection coefficient at infinite time (ρ_∞) as a method of calculating the sample resistance, incorporating it into software for TDR waveform analysis (Heimovaara and de Water, 1993) where V_o and V_{max} (i.e., V_i in Eq. [23]) are illustrated in Fig. 20. The resistance across the rods is then calculated according to

$$R_{tot} = Z_c \frac{1 + \rho_\infty}{1 - \rho_\infty} \qquad [28]$$

where R_{tot} is the total resistance (Ω) of the transmission line, Z_c is the cable tester impedance (50 Ω), and ρ_∞ is the reflection coefficient at infinite time on the waveform, or at a point where the reflection level has stabilized to a maximum value. The Tektronix TDR has a useful feature in which the resistance (Ω) value at any given apparent distance along the transmission line can be read directly at the location of the cursor. Friedman and Jones (2001) used this feature to characterize qualitatively the dependence of the electrical conductivity's anisotropic factor on distance in the time domain, which relates to frequency.

Heimovaara and deWater (1993) further proposed that the total resistance was made up of two components, that of the cable (R_c) and that of the sample (R_s):

$$R_t = R_s + R_c \qquad [29]$$

However, more recently Castiglione and Shouse (2003) demonstrated that this intuitive relationship is inexact. They presented a new procedure to calculate the sample resistance (R_s), independent of contributions from cable and fittings, that requires the waveform to be scaled according to the reflection coefficient for an open circuit (ρ_{open}) in air and for a shorted circuit (ρ_{short}):

$$\rho_{scaled} = 2\frac{\rho_{sample} - \rho_{open}}{\rho_{open} - \rho_{short}} + 1 \qquad [30]$$

The value of ρ_{scaled} is now used in Eq. [28] in place of ρ_∞ to determine the sample resistance. Making good repeatable measurements for the open and short are difficult using conventional TDR probes, and specialized calibration kits have been used for precision work in this regard (Feldman et al., 1996; Huisman et al., 2002). The bulk EC for a given temperature depends on the cell constant, or geometric factor (g) of the probe conductors (discussed in more detail in the following section), and is
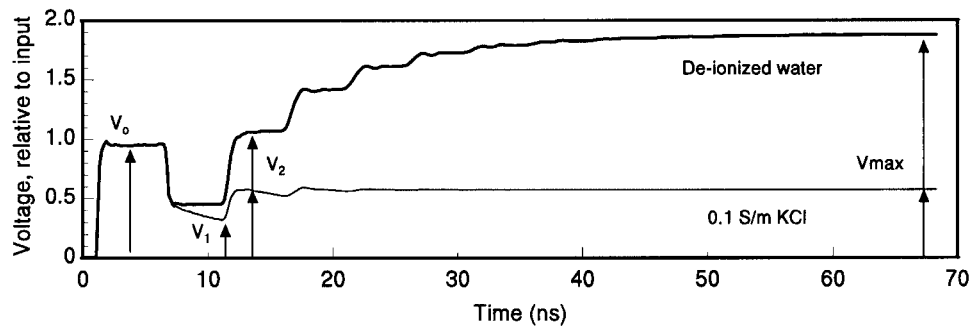
Fig. 20. TDR waveforms from deionized water and from a KCl solution. The various voltages used to obtain the reflection coefficient are illustrated.

$$\sigma_{dc} \ (S \ m^{-1}) = \frac{1}{R_s \ (\Omega) \ g \ (m)} \qquad [31]$$

In most circumstances, when $R_c \ll R_s$, Eq. [29] is adequate for measurements of EC in soils.

The Broad-Band Conductivity Method of Topp, Yanuka, Zebchuk, and Zegelin

The method described above allows one to obtain a measurement of the low-frequency EC. However, conductive losses occur at a range of frequencies. Thus, Topp et al. (1988) proposed an alternative method of estimating what is best described as a broad-band conductivity term. According to Topp et al. (1988) and Topp et al. (2000) the conductivity term (σ_{Topp}) provides an estimate of the combined effects of both the dc conductivity (σ_{dc}) and the imaginary permittivity (ε_r'') due to relaxation losses.

$$\sigma_{Topp} = \omega\varepsilon_o\varepsilon_r'' + \sigma_{dc} \qquad [32]$$

Topp et al.'s (1988) expression was given in terms of voltages in Nadler et al. (1991) as

$$\sigma_{Topp} = \frac{\sqrt{\varepsilon_r'}}{120\pi l} \ln\left[\frac{V_1(2V_0 - V_1)}{V_0(V_2 - V_1)}\right] \qquad [33]$$

with l as the physical length of the probe (m). The voltages with reference to the waveform are illustrated in Fig. 20. One can see that for deionized water the signal is horizontal; however, the equivalent signal for KCl slopes down to V_1. This divergence of the signal from the horizontal is considered to be caused by attenuation of the signal as it propagates along the length of the probe. As the attenuation depends on both the EC of the material and its dielectric relaxation properties, this broadband conductivity term may capture effects of both dielectric losses and conductivity for the TDR frequency bandwidth. Interpretation of the waveform in this way is interesting but should not be considered equivalent to measurements with low-frequency techniques such as a bridge or four-probe instruments.

PROBE DESIGN, CONSTRUCTION, AND CALIBRATION
TDR Probe Design

The aims of optimal probe design are to obtain a representative sampling volume with a robust, practical design while minimizing the effects of EC across the rods. These factors are not complementary, and some compromises must be made in design. For instance, spacing rods further apart increases the ease with which they can be inserted into the soil and increases the magnitude of the resistance measured across the rods. However, it leads to more energy storage closer to the surface of the rods, where, due to compaction effects, the soil might be less representative than undisturbed soil (Rothe et al., 1997).

The previous section suggested the importance of knowing the probe cell constant for determining bulk EC. The following discussion examines approximate ways of evaluating this cell constant and then goes on to examine probe sampling volume, using software to picture the two-dimensional weighting for the sampling volume around probe rods.

Bulk soil EC causes attenuation of the waveform. This has a twofold impact that limits the range in which permittivity can be measured and water content estimated. Some of these effects were discussed by Dalton and van Genuchten (1986). They presented an interesting diagram (Fig. 7 of Dalton and van Genuchten, 1986) comparing maximum waveguide length as a function of both water content and electrolyte conductivity. In the case of their 0.20-m, 3.2-mm-thick rods, spaced 0.05 m apart, they found that at water contents of 0.4 $m^3 \ m^{-3}$ and a solution conductivity of 4 dS m^{-1} the maximum length of probe was about 0.3 m, and at 6 dS m^{-1} about 0.2 m. We found similar results using a TRASE (Soil Moisture Equipment Corp., Santa Barbara, CA) TDR (Skaling, 1992) with 6-mm rods spaced 0.05 m apart. Permittivity measurement was limited to bulk EC values of less than about 2 dS m^{-1} with 0.2-m rods, and about 3 dS m^{-1} using 0.15-m rods. Another effect of increased conductivity is that power is reduced at all frequencies (Fig. 7).

The impact of EC on the TDR measurement depends on the geometry of the probe, specifically its cell constant. More attenuation occurs with long probes with closely spaced rods. The cell constant is essentially the geometric factor g (m) for which values can be approximated for basic geometries of length l, which are based on configurations such as infinite parallel plates, two infinite parallel rods, and an infinite coaxial line (Kraus, 1984).

$$g = \frac{lh}{s} \qquad \text{Infinite parallel plates (m)} \qquad [34]$$

$$g = \frac{12.1l}{\ln\left[\frac{s}{d} + \sqrt{\left(\frac{s}{d}\right)^2 - 1}\right]} \qquad \text{Two rods (m)} \qquad [35]$$

$$g = \frac{2\pi l}{\ln\left(\frac{b}{d}\right)} \qquad \text{Coaxial line (m)} \qquad [36]$$

The greatest error between calculated geometric factors and measured cell constants occurs with parallel plates, as the edge effect is substantial when finite plates are considered. For infinitely long plates ($l \rightarrow \infty$) and for $h/s \rightarrow \infty$ Eq. [34] is exact, and for $h/s \rightarrow 0$ Feynman et al. (1964, p. 6–12) suggested an approximation for g, where one takes the area one *would* get if the plates were extended artificially by a distance 3/8 of the separation between the plates. Equations [34] through [36] also assume no end effects, which of course exist with TDR probes and are more pronounced using shorter rods (Pettinelli et al., 2002). Thus these estimates should not be used as geometric factors for measurement; however, a useful estimate of g can be obtained.

An important consequence of the above analysis method is that one can calculate the effect of increasing or decreasing either rod length or spacing. Decreasing the length of rods decreases g, making them less susceptible to EC interference. However, this also reduces the travel time of the signal and makes measurement of permittivity less accurate. For reasonable field measurement probes between 0.15 and 0.30 m are suggested as a compromise between the accuracy of travel time measurement and conductive losses, as well as ease of insertion into the soil. The effect of spacing is also interesting in that the further apart the rods are the lower the geometric factor. However, increasing the spacing tends to bias the permittivity measurement toward areas closer to the rod surface where there is also likely to be more soil disturbance. Hence it becomes clear that what is beneficial for reducing the effects of EC is detrimental for the measurement of water content.

The Sampling Volume of TDR Probes

The sampling volume of TDR probes has raised much discussion in the literature. Ferre et al. (1998) defined sampling volume as the region of porous material contributing to the TDR measurement; changes in the medium outside this volume have no significant impact on the response of the instrument. It is very helpful to visualize the sampling volume to determine what portion of a soil sample is being measured. Baker and Lascano (1989) endeavored to do this by placing a TDR probe in a collection of glass tubes filled with either air or water. Problems with this approach were pointed out by Knight (1991). Zegelin et al. (1989) examined the voltage distribution around the rods, but it wasn't until

Knight (1992) that the energy density distribution was considered, which effectively relates to the sampling volume in an isotropic homogeneous dielectric media. Knight presented approximate analytical solutions for two-rod (Knight, 1992) and multirod (Knight, 1994) probes. The approach approximates the weighting of the sampling volume energy density distribution, resulting from the solution to the two-dimensional electrostatic problem in the plane perpendicular to the rods. Partial experimental confirmation of these results in soils was presented by Petersen et al. (1995).

The electrostatic potential (ϕ) surrounding TDR rods in the general case, where the effective permittivity (ε_{eff}) varies with position, satisfies

$$\nabla(\varepsilon_{\text{eff}}\nabla\phi) = 0 \qquad [37]$$

The spatial weighting of the sampling volume has the potential (ϕ) satisfying the Laplace equation (for a heterogeneous medium this is a first order-approximation; this is generally assumed for soils):

$$\nabla^2\phi = 0 \qquad [38]$$

The electric field intensity is defined as

$$E = -\nabla\phi \qquad [39]$$

Once the electric field intensity (E) has been determined, the local stored electrical energy per volume is given by

$$W = \varepsilon_{\text{eff}}(\nabla\phi)^2 \qquad [40]$$

where the first-order approximation to the spatial weighting function summed to 1 is

$$w(x,y) = \frac{\nabla\phi_{x,y}^2}{\int_y \int_x \nabla\phi_{x,y}^2 \, dx dy} \qquad [41]$$

Even when the material is assumed to be homogeneous perpendicular to the probe, solving analytically for w can only be done for a few simple geometries.

Knight et al. (1997) presented the use of numerical methods to solve the Laplace equation in two dimensions to model the response of TDR probes. The work considered the role of gaps between the probe conductor and the soil. The findings suggested that small water-filled gaps or partially filled gaps present little problem to TDR measurement. However, small air-filled gaps could have a significant impact on the measurement of the sample relative permittivity. This agreed with earlier work by Hokett et al. (1992), who looked at air- and water-filled gaps between two TDR rods from a practical point of view. Knight's findings compared very favorably with the analytical solutions presented by Annan (1977). This approach has also been used to model a variety of probe configurations (Ferre et al., 1998, 2000; Robinson and Friedman, 2000). The numerical approach offers a powerful tool allowing the modeling of nonuniform probe geometries. It provides visual patterns of the distribution of the relative electric fields, allowing a better conceptual understanding of the measurement. It also offers the advantage of being capable of evaluating the weighting functions of heterogeneous media without the first-order approximation. Software is avail-

able that is specifically designed to perform transmission line calculations such as the Arbitrary Transmission Line Calculator, ATLC (available at http://atlc.sourceforge.net/[verified 5 Sept. 2003]) (Kirkby, 1996). Software commonly used in hydrology, such as Hydrus 2D (Simunek et al., 1994) can also be adapted for the purpose. The electrical problem and horizontal saturated water flow problem are mathematically analogous. The hydraulic head is equivalent to the electric potential (voltage) and the hydraulic gradient is equivalent to the electric field intensity. The energy storage density is then the electric field intensity squared (Eq. [40]). A finite element code commonly used for this analysis is, SWMS-2D for Simulating Water Flow and Solute Transport in Two Dimensional Variably Saturated Media (available at http://www.ussl.ars.usda.gov/MODELS/[verified 5 Sept. 2003]) (Simunek et al., 1994).

Figure 21 demonstrates the analytical solution for a coaxial line, with the relative potential (Fig. 21I, ϕ/ϕ_{max}), field intensity (Fig. 21II, $\nabla\phi/\nabla\phi_{max}$), and energy storage density [Fig. 21III, $(\nabla\phi)^2/(\nabla\phi)^2_{max}$]. These are first-order approximations for the weighting in the perpendicular plane assuming homogeneous permittivity. The analytical solutions are

$$\phi = \phi(r_a) + \frac{Q}{2\pi\varepsilon_o\varepsilon_r}\ln\left(\frac{r}{r_a}\right) \qquad [42]$$

$$\nabla\phi = \frac{d\phi}{dr} = \frac{Q}{2\pi\varepsilon_o\varepsilon_r}\frac{1}{r} \qquad [43]$$

$$(\nabla\phi)^2 = \left(\frac{d\phi}{dr}\right)^2 = \left(\frac{Q}{2\pi\varepsilon_o\varepsilon_r}\right)^2\frac{1}{r^2} \qquad [44]$$

where Q is the charge per unit length, r_a is the radius of the inner conductor, and r is the radial distance up to the outer conductor. The relative field intensity and energy storage are illustrated in Fig. 21 using different colors for contrast.

Diagrams are presented in Fig. 22 for the relative energy storage density for a range of TDR probe configurations, calculated using ATLC (Kirkby, 1996). The calculations assume values of $+1$ and -1 across the TDR rods. The dark areas represent zones of greatest energy storage. Figures 22a through 22d compare the more commonly used TDR probes constructed with rods, whereas Fig. 22e and 22f show cross sections for parallel plate geometries that have been proposed by a number of authors (Chudobiak et al., 1979; Robinson and Friedman, 2000; Inoue et al., 2001).

The literature also contains many novel TDR probe designs, the sample areas of which have been examined in several ways (Ferre et al., 1998, 2001). Figure 23 demonstrates some of these simple designs and the energy distribution around them. The plastic bodies, with a permittivity of 3.3, are represented by the brown color. The yellow represents a homogeneous medium with a permittivity of 10. The upper figure represents a probe that can be placed on the surface of a soil. It is similar in concept to designs presented in Hook et al. (1992) and Selker et al. (1993), both of whom presented probes to be placed on the surface of a material. The diagrams

clearly show how the energy storage and sampling volume in the yellow material, representing soil, is permittivity dependent. The largest sampling volume in the yellow material occurs when it has high permittivity. The next two diagrams show two rods with a plastic tube in between. In the first the angle between the rods is 180° (Maheshwarla et al., 1996), and in the second it is 90° (Redman and DeRyck, 1994). As the permittivity of the insulator between the rods increases more of the energy is stored in this material and less penetrates into the surrounding sample to be measured. The final diagram considers two parallel plates with a plastic-filled gap in between the plates; this is a similar concept to the one used by some profiling TDR probes (Hook et al., 1992; Sun et al., 2000; Wright et al., 2001).

Comparison of Probe Designs

Two-Rod vs. Three-Rod Probes

Two-rod and three-rod probes are most commonly used for routine field work. As a result, many studies have examined the attributes of these probes (Dalton and van Genuchten, 1986; Zegelin et al., 1989; Knight, 1992; Ferre et al., 1996). Ferre et al. (1998) conducted a theoretical study comparing the sampling volume of balanced two- and three-rod probes in some detail. They found that given an increase in rod diameter for the same center spacing a marginal improvement in the uniformity of the distribution of the sensitivity within the sample area was achieved. In comparison, the three-rod probe had a reduced sample area and more energy around the central rod. We therefore would suggest that the two-rod probes are perhaps preferable for fieldwork.

One of the discussions in the literature centers round the need to use a balun to balance the transmission line signal (Zegelin et al., 1989). On a balanced transmission line the two conductors carry opposite polarities that are equal with respect to ground (e.g., $+1$ V, -1 V). In the case of an unbalanced line the voltages are unequal (e.g., $+1$ V, 0 V), an example of an unbalanced line is a coaxial cable. Initial studies using TDR tended to use a balun to balance the line (Topp et al., 1982a, 1982b); however, Zegelin et al. (1989) suggested that unbalanced probes could be used with little or no loss of precision. A definite advantage of omitting the balun is that bulk soil EC can be determined from a TDR waveform.

Most of the papers presented in the literature that discuss probe sampling volume show diagrams for the balanced case (Knight et al., 1997; Ferre et al., 1998). In practical terms Zegelin et al. (1989) found this made little difference to measurements. More recently this issue has been raised again by Mojid and Cho (2002) who suggested that travel time and hence permittivity measurement differ depending on which rod is connected to the core. In experiments presented by Nissen et al. (2003) and in measurements of our own, we found no difference in travel time. However, the energy content of the signal does change. Figure 24 presents waveforms collected with a Tektronix cable tester using a 0.5-m-long two-rod probe. The head of the probe was
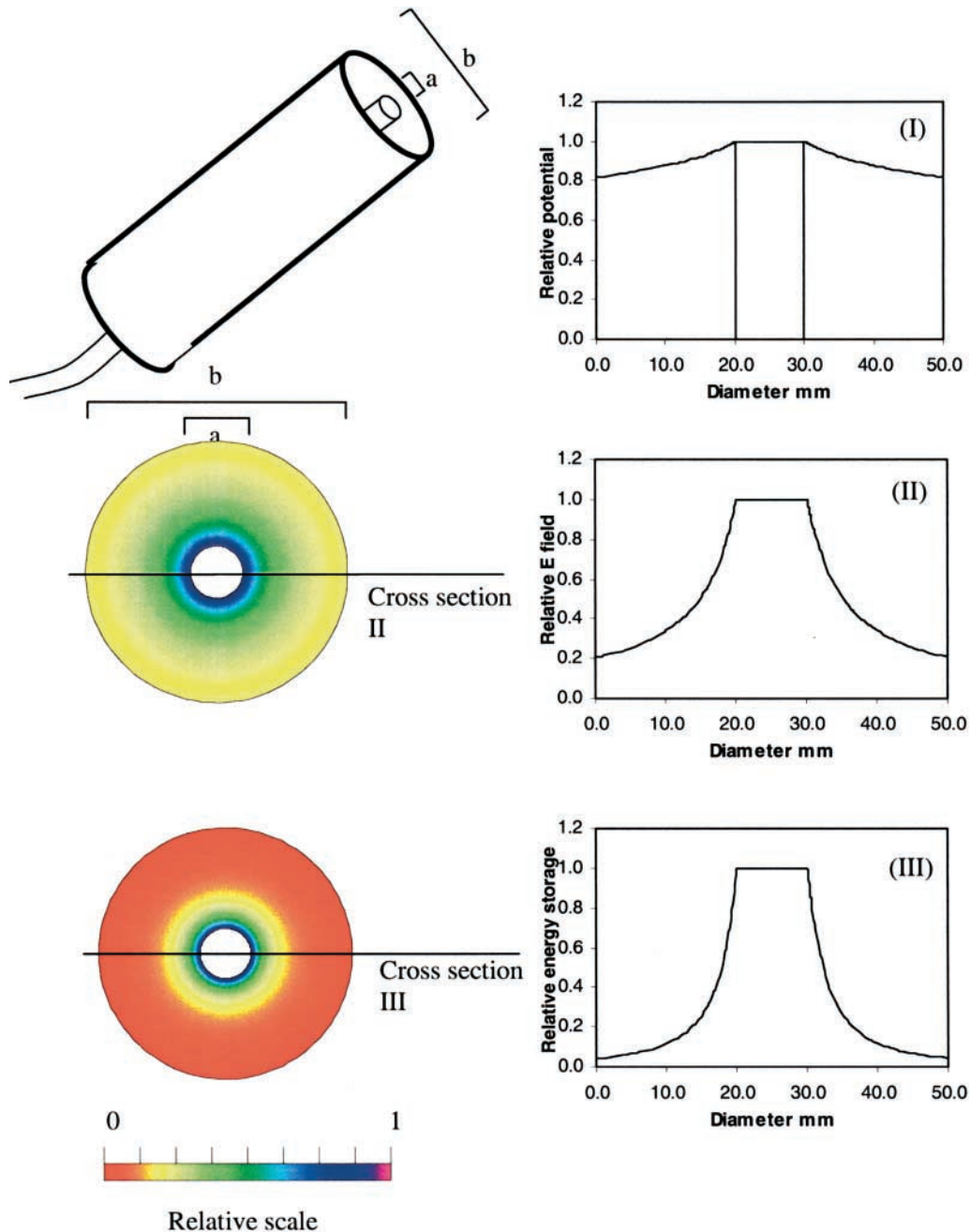
Fig. 21. Electrical fields in a coaxial cell. Panels I, II, and III show the progression from the relative electrical potential through the relative electrical field intensity to the relative electrical energy storage density, respectively. The graphs correspond to the marked cross section.

designed so that the probe head could be reversed without changing the location of the probe rods. The waveforms in air and water lie on top of each other regardless of which way around the probe head is connected to the probe rods. However, when one rod is half submerged in water and half in air, the amplitudes of the waveforms differ, depending on which rod is connected to the core of the coaxial cable. When the rod connected to the core is in the water the waveform is lower in magnitude than the other way around. This indicates that more energy is contained in the water when the core is connected to this submerged rod. Since these results indicate that there was no difference in travel time, it is likely

that the results presented by Mojid and Cho (2002) either resulted from to the use of shorter probes or were affected by having to disturb the rods during the measurements.

Comparison between Probes Using Plates or Rods

One of the main aims of TDR probe design is to try to obtain a relatively uniform energy distribution in the sampling volume. Achieving this aim reduces the bias of the measurement for areas close to the surface of the rods where disturbance of the porous medium will be maximal. Figure 25 compares the relative energy storage

a) 2-rods   b) 3-rods   c) 3-rods

d) 5-rods   e) 2-plates   f)2-plates
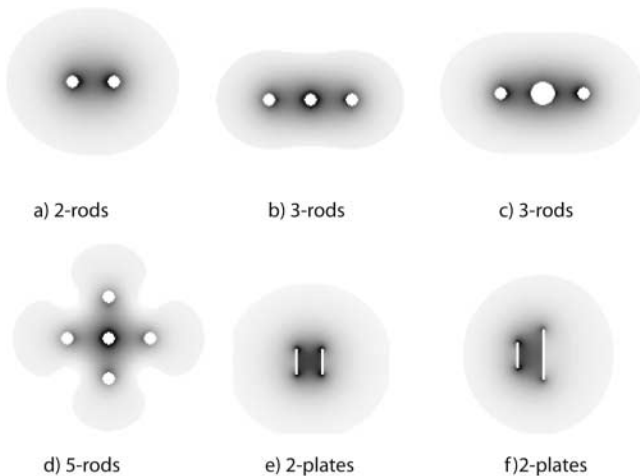
Fig. 22. Relative electric field intensity and energy storage density cross-sections for a variety of TDR probe designs. Configurations include (a) two rods, (b) three rods, (c) three rods with the center rod twice the diameter of the outer rods, (d) five rods, (e) parallel plates, and (f) parallel plates with the right-hand plate twice the length of the left-hand plate.

density between two balanced parallel rods and two balanced parallel plates. The diagrams illustrate that more of the energy is closer to the conductor using rods than using plates. Chudobiak et al. (1979) first suggested the use of TDR probes with a plate geometry. More recently plates acting as blades have been proposed for both static (Robinson and Friedman 2000) and mobile (Inoue et al., 2001) TDR measurements. Robinson and Friedman (2000) conducted a comparison of four different probe geometries, comparing plates vs. rods with two- and three-conductor geometries. These included two parallel rods, three parallel rods, two parallel plates and three parallel plates. The three rods were constructed from 4-mm-diam. stainless steel, 0.15 m long, with a center spacing of 24 mm between outer and inner conductors. The plates were made from 2-mm-thick stainless steel, 20 mm high and 0.15 m long, with centers spaced 22 mm apart. Two replicates of each probe were installed horizontally at a depth of 0.1 m in a loamy sand experimental plot. They were installed in wet soil that was then dried, rewetted, and dried again. A subsequent rewetting by flooding followed by drying was performed, and measurements of permittivity were simultaneously made for all probes. Results suggested that at least one wetting and drying cycle was required for the probes to settle in the ground. The estimated water content, using Topp's universal equation (Eq. [46]), for the set of measurements is presented in Fig. 26. The narrower spread of the estimated water contents among the four types of probe clearly demonstrates improved measurement precision using plates instead of rods. However, the plates can be more difficult to install and they are only suitable for nonsaline soils with low bulk EC due to a high geometric factor causing rapid waveform attenuation.

Installation of Probes for Field Work

The installation of TDR equipment in the field has received considerable attention in the literature (Topp et al., 1982b; Topp and Davis, 1985a, 1985b; Cassel et al., 1994). One of the principal concerns is how to correctly install the probes and cause the least amount of disturbance to the soil. The 12.7-mm-diam. rods used in Topp and Davis (1985b) were pushed into 9.6-mm pilot holes. However, they state in the same paper that they found no pilot holes were necessary when using 6- or 3-mm-diam. rods. More recently a comprehensive study was made for the installation of the TRIME (IMKO GmbH, Ettlingen, Germany; IMKO, 1996) TDR probes. These differ slightly from more conventional probes as they have a PVC coating around them, although the authors claim the results are comparable with conventional probes. In their work they compared installation by pushing the rods into the soil and by inserting the rods into pre drilled pilot holes. Their probes had 3.5-mm-thick rods and 8.0-mm-thick rods. The 8.0-mm-thick probes that were pushed into the soil created substantial compaction, which resulted in a 10% underestimation of the water content. In their conclusions they recommend predrilling holes for rods with diameters larger than 6 mm. One of the concerns about using pre-drilled holes is ensuring that these holes are not too long. Gregory et al. (1995) presented a study examining the errors associated with having a space at the tip of a vertically inserted probe. Some of their results are presented in Table 1 and demonstrate more substantial underestimation of water content with shorter probes. The error appeared constant with a gap of about 10 mm or larger.

A further issue concerning installation is the choice of vertical or horizontal placement in the soil. Sometimes horizontal placement is preferred for obtaining better depth resolution. Practical experiments conducted by Nadler et al. (2002) appear to confirm that averaged water content values from horizontally installed probes and vertically installed probes showed little deviation. A pragmatic solution to obtaining better depth resolution from vertically installed probes is to use a profiling probe (Hook et al., 1992; Sun et al. 2000). A combination of modeling and measurements presented by Timlin and Pachepsky (2002) showed that a vertically installed probe could be used to accurately follow infiltration into the soil. They used a waveform simulation model fitted to the measured waveforms to calculate the depth of water infiltrated. The choice of vertical or horizontal installation therefore comes down to the accuracy of depth resolution required vs. how much soil disturbance can be tolerated by digging a horizontal trench. Under some circumstances it may be beneficial to install probes at 45° to minimize disturbance from digging a trench while still allowing measurements down the soil profile.

Construction of TDR Probes

Time domain reflectometry probes may be constructed in-house or purchased from commercial vendors. Advantages of fabricating probes include lower cost and the ability to customize probe design and dimensions. A primary advantage of commercial probes is convenience, particularly for those lacking facilities or materials required for routine probe fabrication. However,
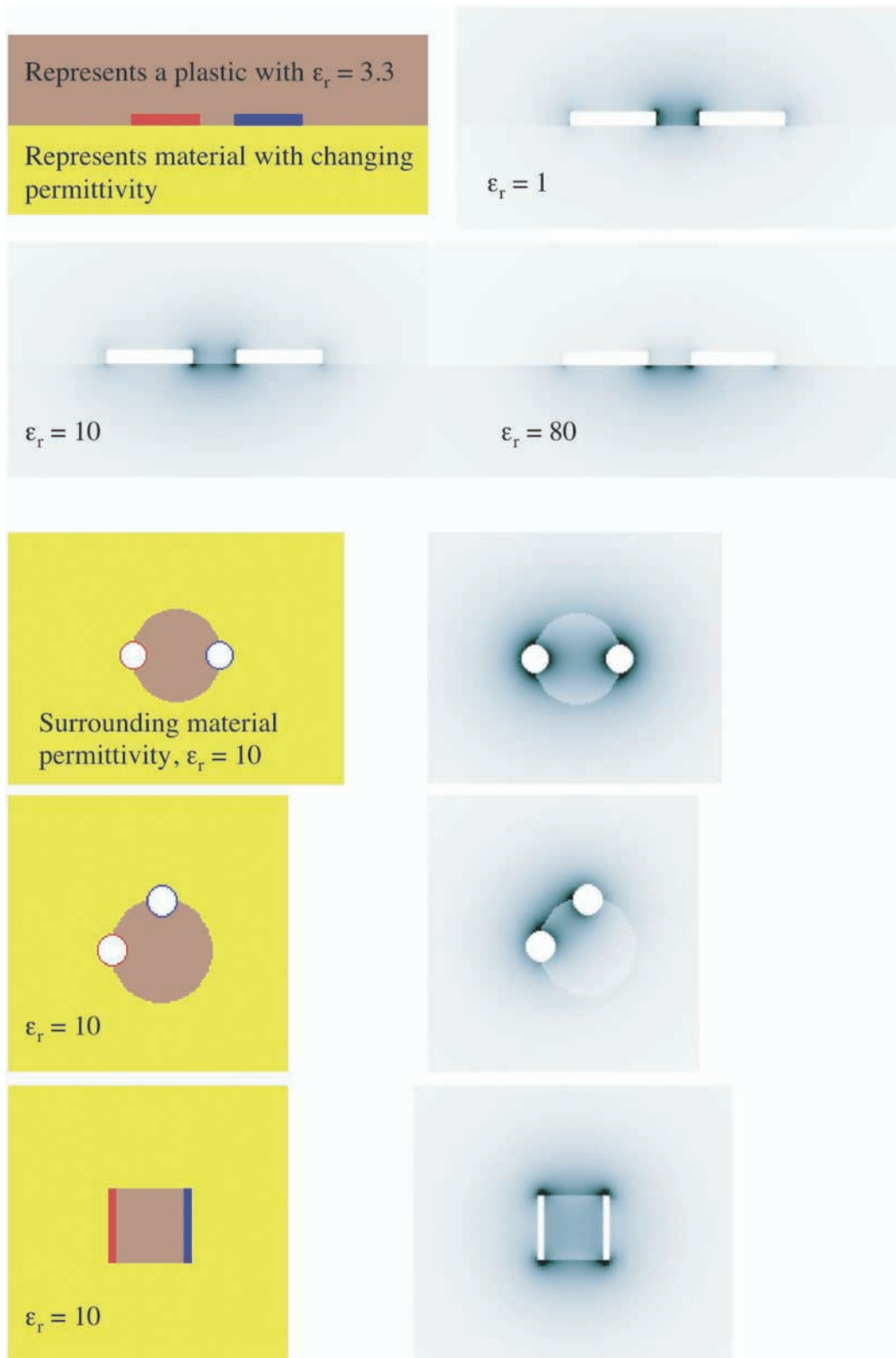
Fig. 23. Four alternative probe designs. The red represents the positive rod and the blue the negative. Upper panels show the change in sampling volume as a function of permittivity. The brown areas represent a permittivity of 3.3 for PVC, and the yellow areas represent a permittivity of 10, common for unsaturated soils.

homemade probes allow for designs to match specific applications. Baker and Goodrich, (1987) presented a design for combined TDR and thermal conductivity measurements. Since then a number of others have developed probes combining these measurements (Noborio et al., 1996; Ren et al., 1999; Ochsner et al., 2001).

Fig. 24. Waveforms collected from a two-rod parallel probe with both rods in air, both rods in water, and then one rod in air and one rod in water. One rod was connected to the inner conductor of a coaxial cable and the other to the outer sheath; this was then reversed. In air and water this made no difference. However, the waveform magnitude is affected depending on which rod is connected to the inner conductor of the coaxial cable and the dielectric that rod is in. The travel time remains unaffected.
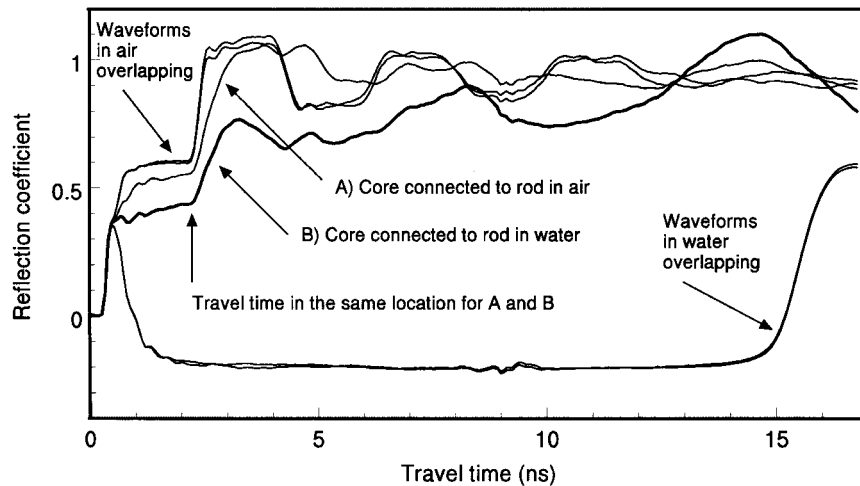
Or and Wraith (1999a) used a TDR probe as the basis of a matric potential sensor using porous disks with differing pore sizes placed along the probe. Other workers have presented contrasting designs for simultaneous water content and potential measurement using the same probe (Baumgartner et al., 1994; Noborio et al., 1999; Vaz et al., 2002). The relationship between soil strength and water content is complex, and Topp et al. (1996) proposed a combined TDR and penetrometer as an instrument for exploring this relationship (Young et al., 2000). An alternative design was presented in Vaz and Hopmans (2001), with results in Vaz et al. (2001). At times it is not easy or desirable to insert long probes into a material. The use of short probes does compromise the travel time for the signal; however, Persson and Wraith (2002) proposed a shaft-mounted sensor. This has the equivalent of a 0.2-m probe wrapped around a 30- to 40-mm-long shaft. Noninvasive probes have also been suggested as a way to overcome the problem of insertion, such as the profiling probe proposed by Ferre et al. (1998, 2003) for use in two parallel access tubes. Selker et al. (1993) proposed a noninvasive TDR probe design, with similar designs having been proposed for column studies (Nissen et al., 1999). Heavy-duty probes
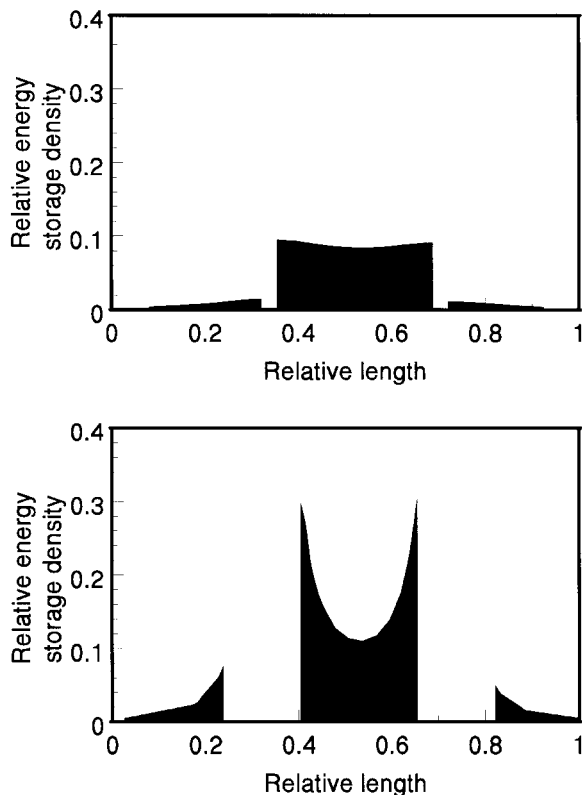
Fig. 25. The relative energy storage distribution ($\nabla\phi^2$) cross sections from between (a) parallel plates and (b) twin rods. The graphs indicate that there is a more even distribution of energy in the sample between plates than between rods.
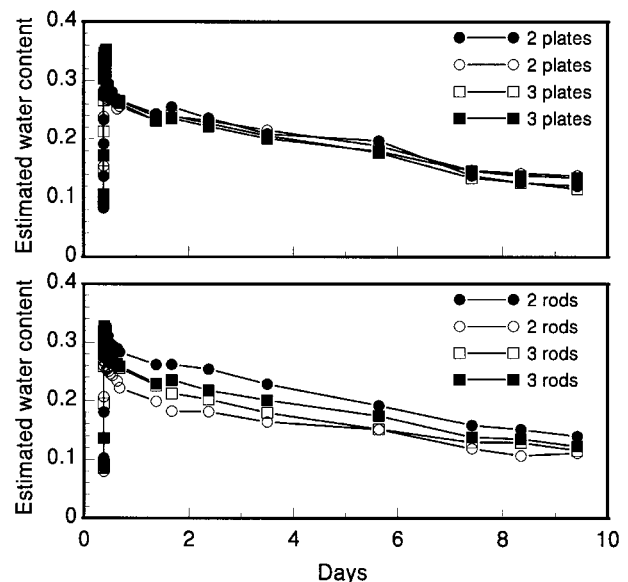
Fig. 26. A comparison of water content measured during a field drainage experiment using probes constructed from plates (upper diagram) and probes constructed from rods (lower diagram). (From Robinson and Friedman, 2000.)

Table 1. Data from Gregory et al. (1995) showing the effect of a cavity under the probe tip. The negative sign indicating water content underestimation compared with good probe tip soil contact.

Probe length	Cavity length			
	5	10	15	20
m	mm			
0.1	−0.004	−0.011	−0.012	−0.011
0.2	−0.010	−0.014	−0.012	−0.016
0.3	−0.005	−0.011	−0.010	−0.010

are often required for field use where repeated insertion is required (Long et al., 2002).

Some proprietary waveform analysis software algorithms require an impedance mismatch or an alternative electrical marker to signal the start point for travel time analysis, and these probe designs may be somewhat more difficult to fabricate. Materials for conventional probe designs include a suitable coaxial cable (generally 50-Ω RG-58A/U or RG-8A/U), BNC plug connector to match the coaxial cable, rods or plates to form the probe transmission line, and epoxy or other casting material to form the probe head. A 75-Ω coaxial cable, which is easily available because of its use with television antennas, also works well for water content measurement, but it can complicate measurement of EC. Cables can often be fitted with either BNC connectors or the slightly more expensive N-type connectors. The difference is the frequency limit. For BNC this is about 1 GHz, and for N type it is about 10 GHz. As a high-frequency signal travels at the surface of a metal, gold-plated connectors give optimal performance, but the improvement in performance rarely justifies the cost. Stainless-steel welding rod works well for probe construction. The particular alloy makes little practical difference. We have found 316L works well.

There are many potential ways to build serviceable TDR probes. We will briefly describe a method that has worked well for us for several years. Coaxial cable may be purchased in quantity on rolls or spools and cut to desired length. Insulation at the probe end is stripped back 10 mm or more to access the signal and shield wires and to provide sufficient length to accommodate the desired rod spacing. A jig (Fig. 27) or form is required
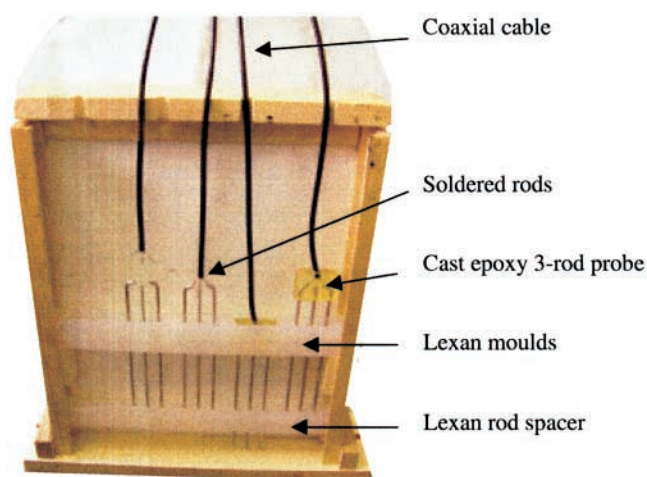
Fig. 27. Time domain reflectometry probe construction jig.

to cast the probe heads where the coaxial cable attaches to the rods. We use machined polypropylene molds in a wooden jig in which the epoxy resin is cast. Holes matching the rod diameter and spaced appropriately (Knight, 1992) are drilled through the base of the jig, with adjacent probe heads separated. Shrinkage of the epoxy in polypropylene molds facilitates release of the probe head. In other mold materials, petroleum jelly may be used to cover the inside surfaces, so the epoxy will release from the mold. Rods are placed through the drilled holes, and coaxial cable signal (central conductor) and ground (outer sheath) are soldered to the rod ends. Silver solder and an appropriate flux should be used for stainless-steel rods. For unbalanced two-rod probes, the signal is attached to one rod, and grounded to the other. An impedance matching transformer (balun) may be used (Spaans and Baker, 1993) if a balanced signal is required, but as discussed above, this is not essential. For coaxial emulation probe designs with three or more rods, the signal is attached to the center rod, and the shield split to the outer rods. After the rods are affixed to the cable, they may be pulled down into the channel so that about 10 to 15 mm of the rod ends will be covered in epoxy, with another 5 mm or so above the rod ends to secure the coaxial cable and junctions. Rods may be cut to exact length before fabrication, or to approximate length and then trimmed after the probes are formed. Epoxy may be poured into the headspace. Care should be taken not to cover rod ends with lubricant, as this would preclude effective bonding of rods to the epoxy head material. We use a marine epoxy resin (epoxy resin and hardener, System Three Resins, Inc., Seattle, WA). Several analogous products are available, but note that the material selected must be impervious to water. In cases of extreme temperature changes, expansion or contraction of the dissimilar materials (i.e., rod and epoxy) may allow water to enter or the probe head may crack. After allowing the resin to cure, the probes are removed from the jig. The head may be abraded to smooth any rough edges, and rods may be cleaned with a scraper and/or solvent if required (being careful not to weaken the epoxy head). We shape the ends of our rods to a pointed cone using a grinder to facilitate insertion. This may be done before or after probe fabrication, but is more easily accomplished initially (if rods are cut to exact length). The final step is to affix the BNC connector to the opposite end of the coaxial cable. Several types of BNC connector are available, in terms of the manner in which they attach to the cable, including crimp, twist, and solder. We find the latter to be substantially superior in terms of physical and electrical integrity.

Commercially Available Probes

Time domain reflectometry probes in a variety of configurations may be purchased from several vendors, including Campbell Scientific, Inc. (Logan, UT); Dynamax, Inc. (Houston, TX); ESI Environmental Sensors, Inc. (Victoria, BC, Canada); Soil Moisture Equipment Corp. (Santa Barbara, CA), TRIME (Ettlingen, Ger-

Table 2. Comparison of different TDR devices and features.

TDR features	Tektronix 1502(B,C)†	Easy Test FOM/mts†	Soil Moisture Mini Trase† 6050X3	Environmental Sensors Inc. MP-917†	Campbell Scientific TDR100†	Soil Moisture Trase System I† 6050X1	Mesa Systems TRIME FM2†
Transmitted signal rise time, ps	200	200	125–155	>200	170	125–155	300
Output pulse amplitude, V	0.30	2	1.6	0.3	0.25	1.6	
Weight, kg	6.5	3.8	3.4	5	0.7	12	0.9
Size, cm	$44 \times 32 \times 13$	$26 \times 18 \times 13$	$23 \times 20 \times 13$	$27 \times 25 \times 17$	$21 \times 11 \times 6$	$28 \times 42 \times 23$	$18 \times 8 \times 6$
Cost ($, minimal to use)‡	11 695	4707	6895	5350	3650§	9550	4370
Probe compatibility	Generic	Proprietary	Generic	Proprietary or generic	Generic	Generic	Proprietary
Display options	LCD, PC	LCD, PC	PDA, PC	LCD, PC	PC, DL§	LCD, PC	LCD, PC
ε–θ calibration	None	Fixed	User defined	Fixed	User defined	User defined	User defined
Device output‡	WF	EC, θ, T	WF, ε, θ	WF, θ	WF, EC, ε, θ	WF, ε, θ	WC
Waveform size, pixels	251		1200	255	100–2048	1200	
Storage options‡	PC, DL	PC	PC, DL, PDA, IS	PC, DL, IS	PC, DL	PC, DL	PC
Electrical conductivity	Manual	Yes	No	No	Yes	No	No
Cable connection type	BNC	BNC	BNC	BNC	BNC	BNC	Proprietary
Reported accuracy, %FSO¶	±1	±2	±2	±1	±1	±2	±1
Power supply‡	AC, battery	AC, battery	AC, battery	AC, battery	Battery	Battery	Battery
Analysis software	TDRANA, WINTDR, TACQ	Proprietary	WinTrase, TraseTerm	View-Point	PCTDR, WINTDR	WinTrase	IMP232 Micronet

† Tektronix Inc., Beaverton, OR, www.tektronix.com; Easy Test Ltd., Lublin, Poland, www.easytest.lublin.pl; Soilmoisture Equipment Corp., Goleta, CA, www.soilmoisture.com; Enviro Sensors, Victoria, BC, Canada, www.esica.com; Campbell Scientific Inc., Logan, UT, www.campbellsci.com; Mesa Systems Co., Medfield, MA, www.mesasystemsco.com.

‡ Prices verified July 2003.

§ The TDR100 is designed for use with a datalogger (price not included) but can function manually using PCTDR software. Interface using WINTDR software may be available in 2004.

‡ WF = waveform, θ = water content, ε = permittivity, EC = electrical conductivity, T = temperature, DL = datalogger, PDA = personal digital assistant, IS = internal storage, AC or DC = power option.

¶ %FSO is percentage of full-scale output.

many), and others. Note that some of these probes may be specific to commercial or proprietary TDR measurement systems; see Table 2. Cost varies widely, depending on the particular system and probe.

TDR Probe Calibration and Permittivity Measurement

Obtaining an exact measurement of the travel time is crucial to permittivity measurement from a TDR waveform. High quality waveforms make it easier to measure the travel time more accurately. This depends on two things: the physical construction of the probes and the homogeneity and relaxation behavior of the dielectric material. A series of waveforms are presented in Fig. 28 for dielectric fluids with negligible relaxation occurring in the TDR frequency range. The waveforms have dis-

tinct reflections, from which the travel time can be accurately measured. As a comparison two alcohols are presented in Fig. 29—ethanol with less relaxation has a more distinct end reflection than octanol, which is more rounded due to strong relaxation in this frequency bandwidth (see also the propanol–water waveforms in Fig. 9). The highly rounded octanol waveform is typical of a dispersive material with relaxation in the measurement frequency bandwidth as previously discussed in the section on interpreting and modeling waveforms. This is important because poor probe construction can also lead to dispersion and filtering out of the higher frequencies and thus more indistinct, rounded waveforms.

Each probe requires length calibration to maximize accuracy of permittivity measurement. An accurate and practical method is to calibrate probes in air and water (Heimovaara, 1993; Robinson et al., 2003). Analysis soft-
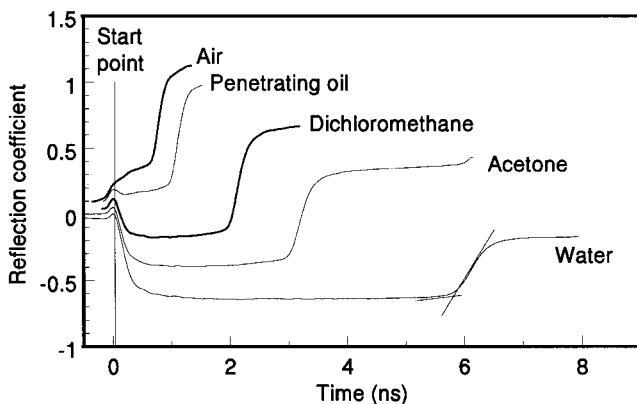

Fig. 28. A series of waveforms collected in a coaxial cell demonstrating how the waveform travel time increases as the permittivity increases. Tangent lines are fitted to the water waveform, the intersection being the point from which the time is measured.
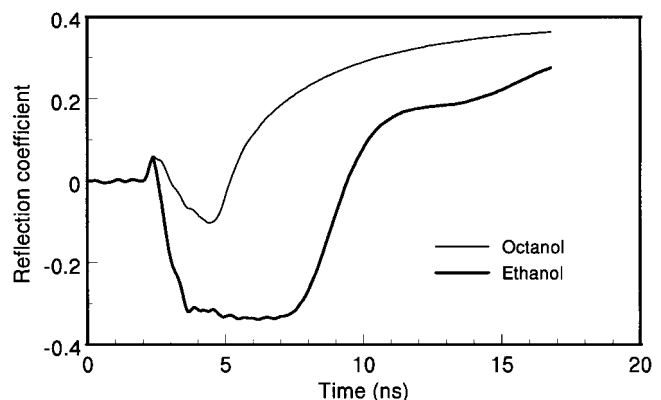

Fig. 29. Waveforms in ethanol (ε_s = 22) and octanol (ε_s = 10) demonstrating the rounding of a waveform that contains relaxation in the TDR frequency bandwidth (Octanol).
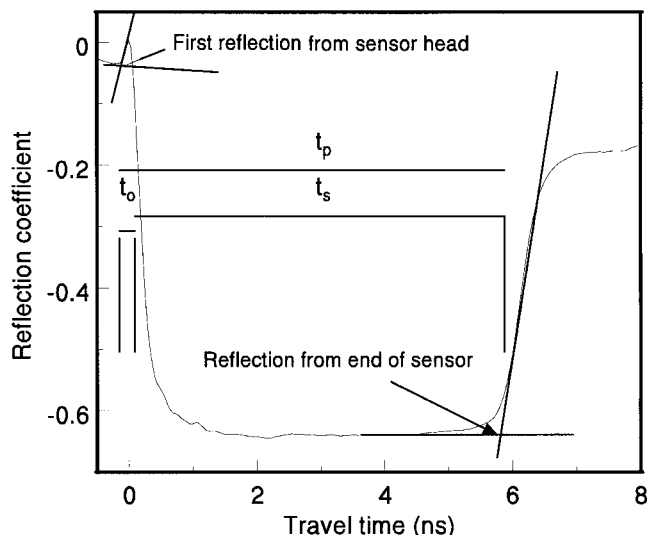
Fig. 30. An example of a waveform in water showing tangent lines fitted at the end of the waveform and the times used to calibrate a TDR probe (Eq. [45]).

ware was presented by Heimovaara and deWater (1993) that locates by fitting tangents the base of the bump (first reflection of signal) created by the impedance mismatch between the cable and sensor head (Fig. 30). It then locates the second reflection from the end of the sensor, denoted "reflection from end of sensor" in Fig. 30. The time between these two points is denoted as Δt_p (Fig. 30). The travel time Δt_p is a combination of the travel time of the signal in the sensor head (Δt_o) and that in the soil surrounding the sensor (Δt_s). Heimovaara (1993) used measurements in air and water, both having known values of permittivity, to obtain both the travel times in the sensor (Δt_s).

$$\Delta t_p = \Delta t_o + \Delta t_s = \Delta t_o + (l_e\sqrt{\varepsilon_r})/c \qquad [45]$$

Two such equations can be solved simultaneously for

air and water so that both l_e (electrical length) and Δt_o can be found. The accurate starting point thereby determined is valid for a fixed temperature and cable length. This method relies on the presence of a bump at the beginning of the waveform caused by the impedance mismatch between the sensor head and cable. This usually occurs since sensor heads tend to have higher impedances than the 50-Ω cable. The base of the bump is a good location reference because it does not move significantly. The work presented in Robinson et al. (2003) showed that in layered systems the apex of the bump, sometimes used as a reference point in other software, would change location.

Many probes are calibrated using only water to determine the electrical length of the probe. The start point is often fixed at the bump apex (B in Fig. 31, right). To demonstrate how choosing an arbitrary start point affects the determination of permittivity an example is presented. In this example the peak of the apex is used as a convenient reference point from which the required travel time is calculated to reach the tangent lines marking the end reflection. We added 0.16 ns to the travel time marked A, and removed 0.10 and 0.26 ns from the travel times, corresponding with C and D, respectively (Fig. 31). The electrical length was calculated according to the permittivity in water and then the permittivity of air was calculated given the respective measured travel time in air using the starting points A, B, C, and D (Fig. 31, right). The estimated permittivity corresponding to these measurements is presented in Fig. 31 in the left panel. Clearly this demonstrates that the apex of the peak is not the legitimate start point, the correct start point lies 0.035 ns to the right of the apex, which was the calculated result using Eq. [45]. The use of any other start point creates an error in the measurement of permittivity, most noticeably at the low permittivity values.

The subject of accurate timing has also been consid-
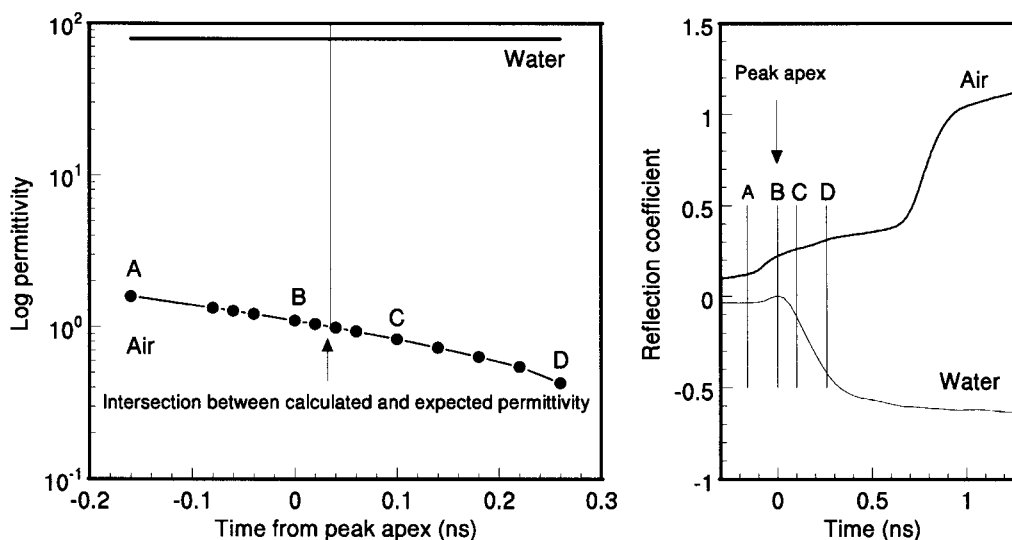
Fig. 31. Left, permittivity estimated from calibration of probe adjusting the electrical length of the probe according to measurements in water using the bump apex as a timing reference. The lines on the right-hand diagram show the corresponding locations on the waveform. The correctly calibrated start point lies 0.035 ns to the right of the point B, the bump apex, according to calibration using Heimovaara's calibration method (Eq. [45]).
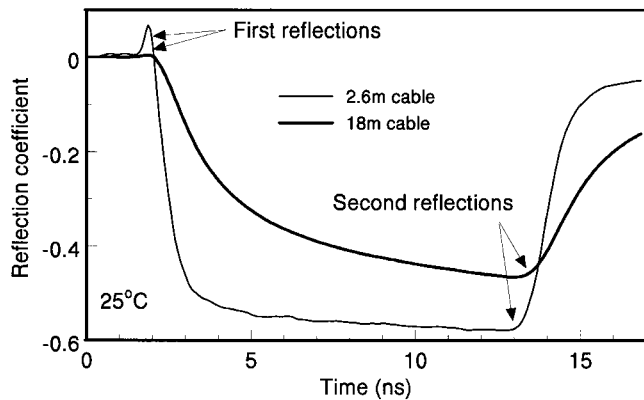
Fig. 32. The response of TDR waveforms to cable length. The longer cable filters the higher frequency components of the signal, and the waveform becomes more rounded.
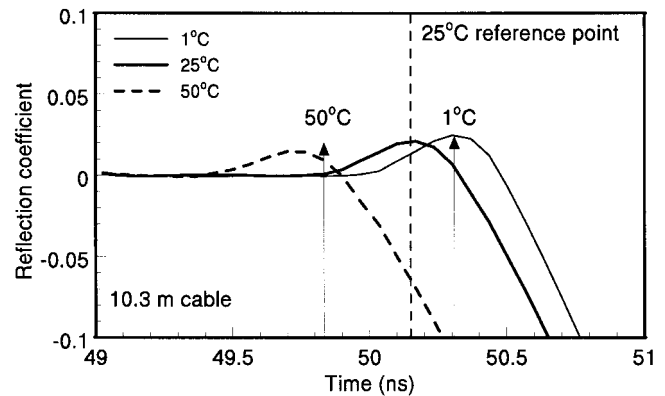

Fig. 33. Influence of temperature in shifting the first reflection peak location resulting from the change in travel time along a 10.3-m cable. Arrows indicate the estimated peak location based solely on the travel time change in polyethylene at 1 and 50°C relative to 25°C.

ered in more pragmatic ways. For example, Hook et al. (1992) developed probes with shorting diodes, which they suggest make finding the probe end reflection easier and reduce propagation velocity errors, making timing measurements more accurate (Hook and Livingston, 1995). These diodes are used to take two measurements, shorted and unshorted. The two waveforms are then differenced to determine travel time. This can be especially useful for measurements in media that is increasingly lossy, before waveform attenuation.

Sometimes it is difficult to locate the position at which the probe begins, particularly for low permittivity materials. To overcome this problem the probes supplied by Soil Moisture Equipment Corp. have an electrical marker in the probe head that causes an impedance mismatch displayed on the waveform as a dip, from which the start of the probe can be located (Fig. 3). The base of this dip also makes a convenient location for fixing the start point for Heimovaara's (1993) method of calculating Δt_o and the electrical length parameter.

Effect of Cable Length and Temperature on Waveforms

The impact of using long cables to connect TDR sensors to the TDR has been considered in a number of experimental studies (e.g., Herkelrath et al., 1991; Heimovaara, 1993). The findings are all similar, showing that increased cable length causes the magnitude of the reflected signal to decrease. This is caused by a decrease in energy as the signal has to travel further down the cables and thus suffers more attenuation. This has a number of impacts, the first of which is that the waveform is altered, causing the first reflection to become less distinct, which can result in problems for software requiring this bump for travel time analysis. The consequences may be an undetectable first reflection and a shift in the analyzed travel time. A further problem is that the second reflection becomes more rounded. This rounding of the waveform is usually associated with dispersion, and in part a filtering of higher frequencies (Logsdon, 2000). An example of the effect of cable length on waveform character for cable lengths of 2.6 and 18.2 m (using the same probe in water) is given in

Fig. 32. A second impact of longer cables regards EC determined using the reflection coefficient. The use of longer cables reduces the reflection coefficient, which means that when probes are calibrated to measure EC they should always be attached to the length of cable that they'll be connected to in the field. Calibration of a probe with a short cable that is to be attached to a long cable in the field will give an erroneous measure of EC, since the probe characteristic impedance used in the calculation of EC will be altered by the cable length. This issue is resolved by using the scaling factors proposed in Castiglione and Shouse (2003) and presented in Eq. [30].

Changes in the ambient temperature of the cable connecting a sensor to the TDR is a further potential source of error that can arise when using long cables. As a cable heats or cools, the propagation velocity of the wave along the cable changes. Problems have arisen when a TDR probe has been calibrated with a fixed start point (first reflection) from which the travel time is measured. As the cable heats and cools, the position of the real start point moves. This is demonstrated in Fig. 33 for a coaxial probe immersed in water. The reference waveform was taken at a temperature of 25°C, and the bump apex can be seen to move relative to this. The shift in the location of the peak is likely a combination of several factors. The most prominent is the change in permittivity of the cable's dielectric material with temperature. For the case of the commonly used cables made with polyethylene as the dielectric, there is a nonlinear reduction in permittivity with increasing temperature. The estimated peak locations based on travel-time change due to temperature-dependent permittivity of polyethylene are shown in Fig. 33. Other factors such as thermal expansion, altered impedance, and measurement accuracy also contribute to the peak shift. This problem is dealt with by automated waveform analysis software such as that of Heimovaara and deWater (1993) or WinTDR (Or et al., 1998), which tracks the TDR waveform using double reflection analysis (see Table 3 regarding analysis software).

Table 3. Features of TDR waveform analysis software packages.

Feature	TDRANA†	PCTDR†§	Viewpoint†	WINTDR†	TACQ¶	WinTrase†
DOS	✓		✓		✓	
Windows 3.x				✓		✓
Windows 95/98		✓		✓		✓
Windows 2000				✓		✓
Windows NT		✓		✓		✓
Proprietary software	✓		✓			
TDR interface capability	1502	TDR100	MP-917	1502/TDR100	1502	6050X1
Cost	$0	$0	$410	$0	$0	$1400
Waveform display	✓	✓	✓	✓	✓	✓
Detection of 1st reflection‡	A, M	A	A	A, M	A	A
Detection of 2nd reflection‡	A	A	A	A, M	A	A
θ analysis‡	A, M	M	A, M	A, M	A	A, M
EC analysis‡	A	A	A	A	A	None
θ, ε, EC, WF storage‡	✓	✓	No EC	✓	✓	No EC
User-defined calib. Eq.	✓	✓		✓	✓	✓
Probe parameter input	✓	✓	✓	✓	✓	✓
Multiplexer control	✓	✓		✓	✓	✓
Waveform averaging	✓	✓	✓	✓	✓	✓
Automated readings	✓	DL req.	✓	✓	✓	✓

† TDRANA, www.frw.uva.nl/soil/software.html; PCTDR, www.campbellsci.com; Viewpoint, www.esica.com; WINTDR, soilphysics.usu.edu; TACQ, www.cprl.ars.usda.gov/programs/; WinTrase, www.soilmoisture.com.

‡ θ = water content, ε = permittivity, EC = electrical conductivity, DL = datalogger, M = manual operation, A = automatic operation.

§ TDR100 performs the waveform analysis internally, PCTDR serves mainly as a laboratory calibration tool.

¶ TACQ operates under a DOS shell in Windows 3.1 or Windows 95.

TDR DEVICES AND ANALYSIS SOFTWARE
Commercial TDR Devices

Since TDR was first utilized for soil moisture measurements in the early 1970s, a host of time domain reflectometers have been introduced, many of which are tailored specifically to soil moisture measurements. The Tektronix 1502B or 1502C metallic cable tester has been the most widely used as a research tool, serving as the reference TDR for almost two decades. As of January 2002, Tektronix no longer produces the 1502B series cable tester, but will continue to service the instrument for several more years and still produces the 1502C. Many newer TDR devices with advanced technology are shown in Table 2, with a comparison of interesting features for TDR measurements of water content and EC. Measurement capability differs among devices ranging in size and weight, with some operating as stand-alone devices capable of remote operation while others must interface with a datalogger or PC for analysis and data collection. System costs vary from just over $3000 to more than $10 000 and the correlation between cost, quality, and functionality is difficult to distinguish without a more detailed evaluation and comparison. Ongoing technological advances provide opportunity for improved pulser technology, with shorter rise time and improved measurement accuracy. An advantage of a faster signal rise time is that it translates to a higher frequency content and less likelihood that the system suffers from low-frequency effects such as those illustrated in Fig. 34 (e.g., Maxwell-Wagner relaxation). The signal rise time, t_r (ps), describes the leading edge of the pulse where most of the energy is contained, and an estimate of its maximum frequency content, f_{max} (GHz), may be computed as shown in Eq. [14] (Strickland, 1970). Benefits derived from higher frequency content and higher power output are realized under attenuating conditions (e.g., long probes, long cables, and high salinity),

where waveform features become indistinguishable and analysis may fail due to signal attenuation and relaxation effects. The transmitted signal rise time and output voltage pulse amplitude reported in Table 2 refer to the direct output of the instrument, neglecting cable or probe losses that occur during a measurement. For most TDR applications in soil science, Hook and Livingston (1995) suggested that a pulse transition time (instrument rise time) of 300 to 400 ps can be used with little sacrifice in accuracy. Other differences among the reflectometers include probe or sensor compatibility and methods of measurement and analysis, as well as storage capability. Probe compatibility is more of an issue for proprietary products, which often require an impedance mismatch

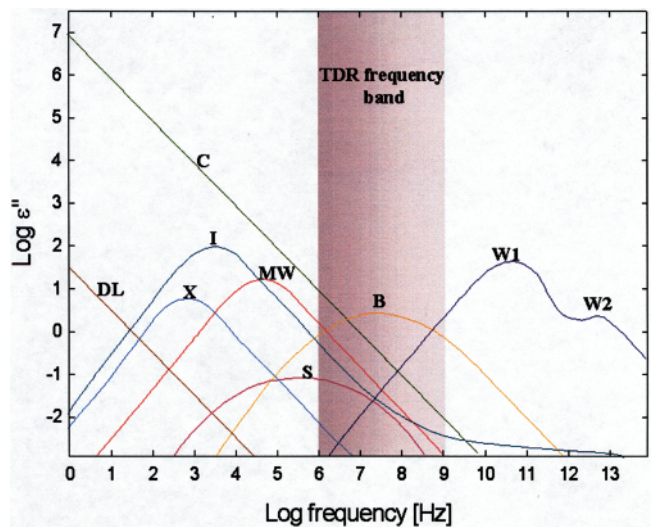**Fig. 34. Contributors to dielectric loss in wet porous media covering a large frequency spectrum. Mechanisms include C, ionic conductivity; DL, charged double layer; X, crystal water relaxation; I, ice relaxation; MW, Maxwell–Wagner relaxation; S, surface conductivity; B, bound water relaxation; W1, principle free water relaxation; W2, second free water relaxation. (Modified from Hasted, 1973, p. 238).**

or shorting diode used by the analysis software to locate the probe. An example of this is the innovative design of a profiling probe (ESI), which uses shorting diodes to provide sectioned measurements of water content within the soil along a single long segmented probe (Hook et al., 1992; Sun et al., 2000). The 1502 and TDR100 devices allow measurement and analysis using generic or custom probe designs while requiring additional operator skills and knowledge. The TDR readout is typically displayed on an LCD screen or PC monitor with numerical output (e.g., permittivity, water content, EC) and in some cases a waveform. Instrument control via remote operation is possible with certain devices (e.g., 1502 via PC or DL [Tektronix], Mini Trase [Soil Moisture Equipment], Trase System I [Soil Moisture Equipment], TDR100 [Campbell Scientific]). Most TDR systems allow user-defined permittivity–water content (K_a–θ) calibration. Output varies widely among instruments, but permittivity is always available as a backward calculation of water content with knowledge of the calibration relationship (e.g., the Topp et al., 1980 equation). Internal storage capacity, as well as battery power, are important features for field measurements. Waveform storage is often optional and can be output at different time intervals in some cases. Waveform size varies among different devices, with some capable of size adjustment, but in all cases the waveform requires considerably more storage space than the typical output of water content and EC. Waveform analysis software is typically incorporated within the TDR unit (TDR100 [Campbell Scientific], TRIME FM2 [Mesa Systems, Ettlingen, Germany], Trase System I [Soil Moisture Equipment], Mini Trase [Soil Moisture Equipment], MP-917 [Environmental Sensors Inc.], FOM/mts [Easy Test, Lublin, Poland]) or it may interface with the TDR as an independent application (1502). Electrical conductivity measurements are supported by only a few of the devices (1502 [Tektronix], TDR100 [Campbell Scientific], FOM/mts [Easy Test]), and this may be a critical consideration for some users. Proper waveform analysis is crucial to accurate determinations of permittivity and EC. For instruments where no waveform is displayed or where users are unfamiliar with common indicators of erroneous waveform analysis, water content measurement errors are more likely to occur. Multiplexer control, allowing multiple probe connection to a single TDR device, is a useful feature for laboratory work and is often a necessity for field applications. A data-logging device is often preferable to a PC for field measurements. Other features that can improve waveform analysis include waveform averaging and smoothing algorithms. In the next section, TDR analysis software features are presented and discussed.

Waveform Analysis Software

Time domain reflectometry waveform analysis software for permittivity (water content) was first automated for applications in soil science by Heimovaara and Bouten (1990) and Baker and Allmaras (1990) using the Tektronix 1502 cable tester. Several of the TDR instruments described above contain internal analysis software (FOM/mts [Easy Test], MP-917 [Environmental Sensors], TDR100 [Campbell Scientific], TRIME FM2 [Mesa Systems]), while others require or allow a PC software interface, where users may perform hands-on waveform analysis and other functions (see Table 3). Nonproprietary software developed for the Tektronix TDR are available at no cost and have the greatest flexibility in terms of waveform analysis for permittivity and EC (Heimovaara and de Water, 1993; Or et al., 1998; Evett, 2000a, 2000b). Key aspects of travel time (waveform) analysis include accurate detection of the first and second reflections leading to consistent and reliable permittivity determination. The first reflection is often marked as a spike or dip in the waveform resulting from an impedance change. This marker may be the result of a diode or balun embedded in the head of the probe, a crimped cable, or simply the impedance change caused by the transition from cable to probe occurring in the probe head. The first reflection point is sometimes identified manually and is used by the analysis software to locate the position of the probe during measurements. Waveform analysis software typically use a tangent fitting procedure to determine the second reflection point, and some software display tangent lines directly on the waveform (e.g., WinTrase, WINTDR; Or et al., 1998). Analysis output varies among different software packages, with all providing water content estimates while some also provide permittivity and EC. Output from the software analysis generally includes time and date as well as permittivity and/or water content and EC where applicable. Probe parameters must be specified (i.e., probe electrical length for permittivity and probe characteristic impedance or geometric cell constant where EC is computed). Not all TDR devices provide EC readings, and only manual readings of EC are available with certain device and software combinations. The waveforms first and second derivatives are often used in automated analyses to identify the second reflection, drawing tangent lines with intersections to mark the location of the second peak (Fig. 30). As the default in most analysis software, the Topp et al. (1980) permittivity–water content relationship is used. User-defined calibration equations are typically linear or polynomial type relationships, but lookup tables for water content are also useful when dealing with clay, organic, or other nonmineral soils.

CALIBRATION EQUATIONS AND MODELS
Empirical Equations

To estimate water content a calibration curve is needed to relate soil volumetric water content, θ, to K_a. Topp et al.'s (1980) seminal paper on TDR presented a number of empirical equations relating soil apparent permittivity to water content. The equation for mineral soils (Eq. [46]) has proven successful in soils that do not contain substantial amounts of bound water, which includes most sands and loams. They also presented an equation for organic soils (Eq. [47]), which differs from mineral soils because of their high porosity and bound

water content (Pepin et al., 1992; Paquet et al., 1993; Schaap et al., 1996).

$$\theta = (-530 + 292K_a - 5.5K_a^2 + 0.043K_a^3) \times 10^{-4} \quad [46]$$

$$\theta = (-252 + 415K_a - 14.4K_a^2 + 0.22K_a^3) \times 10^{-4} \quad [47]$$

In Eq. [46] and [47], θ is the volumetric water content and K_a is the apparent permittivity measured using TDR. A host of additional empirical calibration equations have been presented in the literature (Roth et al., 1992; Jacobsen and Schjonning, 1993), with the primary advance being attempts to incorporate bound water into equations. Perhaps one of the more successful equations was presented by Malicki et al. (1996), who used a sizable data set and a multiple linear regression to develop a relationship, which includes the bulk density (ρ_b) as an additional factor:

$$\theta = \frac{\sqrt{K_a} - 0.819 - 0.168\rho_b - 0.159\rho_b^2}{7.17 + 1.18\rho_b} \quad [48]$$

Simple Mixing Models

The soil can be regarded as a mixture of three dielectric components, air (1), mineral particles (5–10) and water (80), with bound water sometimes being added as a fourth component. Two main modeling pathways have developed regarding mixing models applied in soil science. The first category can be thought of as the power law approximations, which include the so-called refractive index model. The second category makes attempts to develop a more physically based model working from the microscale and building up to the sample scale. The more commonly applied of the latter models are those of de Loor (1968), Dobson et al. (1985), Dirksen and Dasberg (1993), Peplinski et al. (1995), and Friedman (1998). The mixing model approach is more thoroughly discussed in Sihvola (1999).

The power law approximation using a power of 0.5 is commonly used in the soil science literature (Birchak et al., 1974; Whalley, 1993; Heimovaara et al., 1994; Robinson et al., 1999). This model has a simple physical basis for a layered material but does not refer to any of the microstructure of a porous or granular media. A physical derivation for a layered material was presented in the previous section (Eq. [16]). The model presented by Whalley (1993) can be thought of as representing three homogeneous dielectric layers perpendicular to the direction of wave propagation.

$$\theta = \frac{\left(\sqrt{K_a} - 1\right) - \frac{\rho_b}{\rho_s}\left(\sqrt{\varepsilon_s} - 1\right)}{\sqrt{\varepsilon_w} - 1} \quad [49]$$

where the subscripts "s" and "w" denote solid and water, ρ_b is the dry bulk density (Mg m^{-3}), and ρ_s is the density of solid minerals (~2.65 Mg m^{-3}). The bulk density and the solid particle density are related to the soil porosity, ϕ_s, by $1 - (\rho_b/\rho_s)$. Friedman (1997) proposed a $K_a(\theta)$ relationship based on calculating the equivalent capacitance of a three-dimensional solid–water–air capacitor

network that accounts better for the bulk density or porosity of the porous medium.

Physically based models solving the Laplace equation for two-phase EC and dielectric permittivity date back as far as Maxwell (1891) and Maxwell-Garnett (1904), respectively. Within soil science, de Loor (1968) presented a model to describe the effective permittivity (ε_{eff}) of the soil, which considers the soil to be made up of isotropically mixed plate-like particles. Two forms of the model have been presented in the literature, a simplified version with only the three major phases (Jacobsen and Schjonning, 1995) (Eq. [50]) and one applied by Dirksen and Dasberg (1993) (Eq. [51]), which includes bound water:

$$\theta = \frac{3(\varepsilon_s - \varepsilon_{eff}) + 2\phi_s(\varepsilon_a - \varepsilon_s) - \varepsilon_{eff}\phi_s\left(\frac{\varepsilon_s}{\varepsilon_a} - 1\right)}{\varepsilon_{eff}\left(\frac{\varepsilon_s}{\varepsilon_{fw}} - \frac{\varepsilon_s}{\varepsilon_a}\right) + 2(\varepsilon_a - \varepsilon_{fw})} \quad [50]$$

$$\theta = \frac{3(\varepsilon_s - \varepsilon_{eff}) + 2\theta_{bw}(\varepsilon_{bw} - \varepsilon_{fw}) + 2\phi_s(\varepsilon_a - \varepsilon_s) + \varepsilon_{eff}\theta_{bw}\left(\frac{\varepsilon_s}{\varepsilon_{fw}} - \frac{\varepsilon_s}{\varepsilon_{bw}}\right) - \varepsilon_{eff}\phi_s\left(\frac{\varepsilon_s}{\varepsilon_a} - 1\right)}{\varepsilon_{eff}\left(\frac{\varepsilon_s}{\varepsilon_{fw}} - \frac{\varepsilon_s}{\varepsilon_a}\right) + 2(\varepsilon_a - \varepsilon_{fw})}$$

$$\theta > \theta_{bw} \quad [51]$$

where ε_s is solid phase permittivity, ε_a is gas phase permittivity, ε_{fw} is free water permittivity, ε_{bw} is bound water permittivity, θ_{bw} is bound water volumetric water content calculated from $\delta\rho_b S$ assuming a monomolecular layer of tightly bound water of a thickness $\delta = 3 \times 10^{-10}$ m and S is the soil specific surface area (m^2 g^{-1}). The simplified version of the model (Eq. [50]) is more usable for field calibration because it requires only soil bulk density as a physical input parameter, if the water and solid phase permittivities are assumed known. A value of 4.7 has been measured for quartz (Robinson and Friedman, 2003), but a commonly used value for soil minerals is 5 (Dirksen and Dasberg, 1993; Friedman, 1998); the permittivity of free water as a function of temperature (°C) is described by (Lide, 1992):

$$\varepsilon(t) = 78.54[1 - 4.579 \times 10^{-3}(t - 25) + 1.19 \times 10^{-5}(t - 25)^2 - 2.8 \times 10^{-8}(t - 25)^3]$$

$$[52]$$

More recently Friedman (1998) presented an approximate solution (Maxwell-Garnett, 1904) to the Laplace equation for two-phase concentric spheres in a third background phase. He then mixed these in two configurations of solid–water–air and air–solid–water (outwards), and chose a saturation-degree dependent mixture of those configurations that he thought best represented soils. Pore-scale models such as those above are very important and helpful for our understanding and prediction capability of the $K_a(\theta)$ relationship, as are similar approaches presented in other studies (Sen et al., 1981; Sihvola and Kong, 1988; Or and Wraith, 1999b; Jones and Friedman, 2000; Robinson and Friedman, 2001; Jones and Or, 2002; Robinson and Friedman, 2002).

From the standpoint of the typical user who wishes to obtain water content from permittivity measurement, Topp's curve (Eq. [46]) has proven very successful. In heavy clay soils Malicki et al.'s (1996) Eq. [48] might be preferred. The pore-scale mixing models are the best way forward in terms of improving our understanding

of the dielectric properties of porous media and should eventually lead to a comprehensive, physically based mixing model for soil dielectric permittivity as a function of water content.

OTHER METHODS OF WATER CONTENT DETERMINATION

The wide scientific and commercial interest in measuring the water content of porous materials has led to the development of a wide variety of sensing methods and techniques (White and Zegelin, 1995; Gardner et al., 2001; Dane and Topp, 2002; Or and Wraith, 2002), with some practical instrument comparisons presented in Evett (2000c). The gravimetric method is the standard against which other techniques are compared (Gardner et al., 2001); however, it is both time-consuming and destructive. This review has concentrated on TDR, although other techniques exist and may be more suited to certain applications. In the following discussion we group alternative methods into dielectric methods and nondielectric methods. For a comprehensive description of different methods the reader is referred to Dane and Topp (2002).

Dielectric Sensors

Dielectric sensors have become very popular in the last decade primarily because of the highly correlated dielectric–water content relationship, and they can be used near the soil surface, offer high temporal resolution, and are nonradioactive. Measurement of permittivity is an elegant way of estimating water content, and the principal can be applied to measurements at a range of scales, from satellite remote sensing (Jackson et al., 1996; Gardner et al., 2001) to field-scale ground penetrating radar (Huisman et al., 2001) to point measurements (Weiler et al., 1998). The high capital cost of TDR, which has decreased substantially in the last 10 yr, has made room for other low-cost sensors, many of which are discussed by users at the 'Soil Water Content Sensors and Measurement' (SOWACS) web site (http://www.sowacs.com/ [verified 5 Sept. 2003]). Time domain transmission techniques are now commercially available at about a tenth of the cost of a TDR system. These sensors measure one-way travel time, usually around a loop and can have rise times of 200 ps, making them very competitive with TDR, especially for single sensor applications (e.g., ESI, http://www.esica.com/[verified 5 Sept. 2003]; Acclima, http://www.acclima.com/[verified 5 Sept. 2003]; Young et al., 2000). The theta probe (Gaskin and Miller, 1996) is a competitively priced sensor operating at about 100 MHz (Delta T Devices, www.delta-t.co.uk [verified 5 Sept. 2003]). Other impedance devices include Hilhorst et al.'s (1993) low-frequency sensor (20 MHz). Capacitance probes (90–150 MHz) (Bell et al., 1987; Dean et al., 1987; Eller and Denoth, 1996; Paltineanu and Starr, 1997; Gardner et al., 1998; Robinson et al., 1999) tend to be susceptible to soil salinity (Robinson et al., 1998) and less accurate than TDR in terms of permittivity measurement, but offer good solutions in irrigated agriculture, where salin-

ity is low and tracking changes in soil water content is of primary interest.

Nondielectric sensors

Neutron probe

The neutron probe (Greacen, 1981; Bell, 1987; Gardner et al., 2001) is still an important tool for measuring soil water content, especially for profiles of 1 m depth or more and in areas of high soil salinity. The neutron method uses a radioactive source that emits fast neutrons. The neutrons are slowed and deflected primarily by the H atoms in soil water, and a detector in the instrument counts the returning slow thermal neutrons. The number of returning slow neutrons is proportional to the soil water content in mineral soils. The main advantages of the neutron probe are that it has a relatively large sample volume and is very convenient for profiling. However, it has the drawbacks of a radioactive source, a water content–dependent sample volume, the need for calibration for different soils, and that it cannot easily be used near the soil surface.

Dual-Probe Heat Pulse Measurements

Thermal properties (thermal conductivity, heat capacity) of soils are well correlated to volumetric water content because of the disparity between the thermal characteristics of solids, water, and air. The thermal properties are determined using temporal and spatial gradients of temperature (Campbell et al., 1991; Bristow et al., 1994). Constituent heat capacities and thermal conductivities may be averaged to determine bulk estimates, which lead to expressions for inferring volumetric water content from heat pulse measurements. Results of measured thermal conductivity and water content inferred from dual-probe heat pulse measurements (source and sink), show reasonable agreement with model predictions for line source solutions (Kluitenberg and Philip, 1999). Advantages include low-cost and localized measurements that are insensitive to salinity and which have the added capability of making water flux measurements under certain conditions (Ren et al., 2000). Drawbacks to the thermal approach include high sensitivity to geometrical configuration of probes and soil constituents, particle–probe contact sensitivity resulting in reduced accuracy compared with TDR, and a requirement of soil-specific calibration.

SUMMARY

A comprehensive review of TDR technology that applies to the measurement of bulk soil permittivity and EC was presented. The article covers the guiding principles and practical issues, such as TDR probe construction, calibration, and waveform interpretation. The impact of lossy and dispersive dielectrics is discussed. Some of the areas of understanding that present challenges to research might be considered under the following:

1. Improved modeling and inversion of TDR waveforms for extending permittivity and relaxation in-

formation is an area that deserves attention. This is in its infancy but potentially could greatly improve our understanding of the measurement technique and the properties of porous materials. The linkage of such analysis into computer software could provide a very comprehensive TDR waveform analysis package. This approach may also lead to improved permittivity measurement in dispersive dielectrics.

2. Investigating the use of the broadband conductivity to obtain estimates of the imaginary permittivity from waveform analysis would be a very useful contribution. A method of separating real and imaginary permittivity within the measured permittivity is highly desirable. This might greatly improve estimates of water content in clay soils that can have a large imaginary component due to relaxation phenomena.

3. At present probe design constraints limit TDR use for estimating water content to mostly nonsaline soils. However, much of the world's agriculture in semiarid regions occurs in marginal saline areas. Efforts to extend the range of TDR measurements into saline soils are of substantial interest. New and innovative probes are continually being designed and should continue to contribute to the versatility of the TDR technique in the earth sciences.

ACKNOWLEDGMENTS

APPENDIX

List of Greek Symbols

Δt_p	The combined travel time of the TDR signal in the probe head and sensor
Δt_o	The travel time of the TDR signal in the probe head
Δt_s	The travel time of the TDR signal in the sensor
α	Attenuation constant of an electromagnetic wave
β	Phase constant of an electromagnetic wave
β_{cc}	Parameter accounting for a spread in relaxation frequencies (Cole-Cole, 1941) model
δ	Thickness of a monomolecular layer of water approximately 3×10^{-10} m
$\tan\delta$	The loss tangent ($\varepsilon_r''/\varepsilon_r'$)
ε	Permittivity of a material
ε_o	Permittivity of free space (8.854×10^{-12} F m^{-1})
ε_r'	Real part of the relative permittivity
ε_r''	Imaginary part of the relative permittivity
ε_{relax}''	Imaginary permittivity due to molecular relaxation
ε_r^*	Complex relative permittivity

$\varepsilon_{s,cc}$	Static value for the real permittivity (water 80.1 at 20°C)
ε_∞	High frequency limit of the real permittivity (water, 4.22)
ε_s	Solid phase permittivity
ε_a	Gas phase permittivity
ε_{fw}	Free water permittivity
ε_{bw}	Bound water permittivity
ε_{eff}	Effective permittivity of a composite material (mixture)
ϕ_s	Porosity
ϕ	Electrical potential
ϕ_{max}	Maximum value of the electrical potential
γ	Propagation constant for an electromagnetic wave
λ	Wavelength
μ_o	Magnetic permeability of vacuum (1.257×10^{-6} H m^{-1})
μ_r	Relative magnetic permeability
θ	Volumetric water content
θ_s	Volumetric water content at saturation
θ_{bw}	Bound water, volumetric water content
ρ	Reflection coefficient
ρ_∞	Reflection coefficient at infinite time
ρ_{open}	Reflection coefficient at infinite time for an open circuit
ρ_{short}	Reflection coefficient at infinite time for a short circuit
ρ_{scaled}	Scaled reflection coefficient
ρ_s	Particle density of a soil mineral
ρ_b	Bulk density of a soil
σ_{dc}	Direct current equivalent electrical conductivity
σ_{Topp}	Broad frequency band conductivity suggested by Topp et al. (1988)
τ	Variable of integration
ω	Angular frequency ($2\pi f$)

REFERENCES

Annan, A.P. 1977. Time domain reflectometry—Air-gap problem for parallel wire transmission lines. p. 59–62. *In* Report of activities. Part B. Rep. 77-1B. Geol. Surv. of Canada., Ottawa, ON, Canada.

Baker, J.M., and R.R. Allmaras. 1990. System for automating and multiplexing soil moisture measurement by time domain reflectometry. Soil Sci. Soc. Am. J. 54:1–6.

Baker, J.M., and L.E. Goodrich. 1987. Measurement of soil water content using the combined time domain reflectometry-thermal conductivity probe. Can. Geotech. J. 24:160–163.

Baker, J.M., and R.J. Lascano. 1989. The spatial sensitivity of time domain reflectometry. Soil Sci. 147:378–384.

Baumgartner, N., G.W. Parkin, and D.E. Elrick. 1994. Soil water content and potential measured by a hollow time domain reflectometry probe. Soil Sci. Soc. Am. J. 58:315–318.

Bell, J.P. 1987. Neutron probe practice. Inst. Hydrol. Rep. 19. Institute of Hydrology, Walligford, Oxon, UK.

Bell, J.P., T.J. Dean, and M.G. Hodnett. 1987. Soil moisture measurement by an improved capacitance technique: II. Field techniques, evaluation and calibration. J. Hydrol. (Amsterdam) 93:79–90.

Birchak, J.R., C.Z.G. Gardner, J.E. Hipp, and J.M. Victor. 1974. High dielectric constant microwave probes for sensing soil moisture. Proc. IEEE 62:93–98.

Bristow, K.L., G.J. Kluitenberg, and R. Horton. 1994. Measurement of soil thermal properties with a dual-probe heat-pulse technique. Soil Sci. Soc. Am. J. 58:1288–1294.

Campbell, G.S., C. Calissendorff, and J.H. Williams. 1991. Probe for

measuring soil specific heat using a heat-pulse method. Soil Sci. Soc. Am. J. 55:291–293.

Cassel, D.K., R.G. Kachanoski, and G.C. Topp. 1994. Practical considerations for using a TDR cable tester. Soil Technol. 7:113–126.

Castiglione, P., and P.J. Shouse. 2003. The effect of ohmic losses on TDR measurements of electrical conductivity. Soil Sci. Soc. Am. J. 67:414–424.

Chan, C.Y., and R. Knight. 1999. Determining water content and saturation from dielectric measurements in layered materials. Water Resour. Res. 35:85–93.

Chan, C.Y., and R. Knight. 2001. Laboratory measurements of electromagnetic wave velocity in layered sands. Water Resour. Res. 37:1099–1105.

Chudobiak, W.J.B., B.A. Syrett, and H.M. Hafez. 1979. Recent advances in broad band VHF and UHF transmission line methods for moisture content and dielectric constant measurement. IEEE Trans. Instrum. Meas. 28:284–289.

Clarkson, T.S., L. Glasser, R.W. Tuxworth, and G. Williams. 1977. An appreciation of experimental factors in time-domain spectroscopy. Adv. Molec. Relax. Interact. Processes 10:173–202.

Cole, K.S., and R.H. Cole. 1941. Dispersion and adsorption in dielectrics: I-Alternating current characteristics: J. Chem. Phys. 9:341–351.

Dalton, F.N., W.N. Herkelrath, D.S. Rawlins, and J.D. Rhoades. 1984. Time domain reflectometry: Simultaneous measurement of soil water content and electrical conductivity with a single probe. Science (Washington, DC) 224:989–990.

Dalton, F.N., and M.Th. van Genuchten. 1986. The time-domain reflectometry method for measuring soil water content and salinity. Geoderma 38:237–250.

Dalton, F.N. 1992. Development of time domain reflectometry for measuring soil water content and bulk soil electrical conductivity. p. 143–167. In R. Green and G.C. Topp (ed.) Advances in measurement of soil physical properties: Bringing theory into practice. SSSA Spec. Publ. 30. SSSA, Madison, WI.

Dane. J.H., and G.C. Topp. 2002. Methods of soil analysis. Part 4. SSSA Book Ser. 5. SSSA, Madison, WI.

Dasberg, S., and J.W. Hopmans. 1992. Time domain reflectometry calibration for uniformly and non-uniformly wetted sandy and clayey loam soils. Soil Sci. Soc. Am. J. 56:1341–1345.

Dean, T.J., J.P. Bell, and A.B.J. Baty. 1987. Soil moisture measurement by an improved capacitance technique: I. Sensor design and performance. J. Hydrol. (Amsterdam) 93:67–78.

Debye, P. 1929. Polar molecules. Dover Publ., New York.

de Loor, G.P. 1968. Dielectric properties of heterogeneous mixtures containing water. J. Microwave Power 3:67–73.

Dirksen, C., and S. Dasberg. 1993. Improved calibration of time domain reflectometry soil water content measurements. Soil Sci. Soc. Am. J. 57:660–667.

Dobson, M.C., F.T. Ulaby, M.T. Hallikainen and M.A. El-Rayes. 1985. Microwave dielectric behaviour of wet soil Part II: Dielectric mixing models. IEEE Trans. Geosci. Remote Sens. 23:35–46.

Dowding, C.H., and K.M. O'Connor. 1999. Geomeasurements by pulsing TDR cables and probes. CRC Press, Boca Raton, FL.

Eller, H., and A. Denoth. 1996. A capacitive soil moisture sensor. J. Hydrol. (Amsterdam) 185:137–146.

Evett, S.R. 2000a. The TACQ computer program for automatic time domain reflectometry measurements: I. Design and operating characteristics. Trans. ASAE 43:1939–1946.

Evett, S.R. 2000b. The TACQ computer program for automatic time domain reflectometry measurements: II. Waveform interpretation methods. Trans. ASAE 43:1947–1956.

Evett, S.R. 2000c. Some aspects of time domain reflectometry (TDR), neutron scattering and capacitance methods of soil water content measurement. p. 5–49. In Comparison of soil water measurement using the neutron scattering, time domain reflectometry and capacitance methods. IAEA-TECDOC-1137. IAEA, Vienna, Austria.

Feldman, Y., A. Andrianov, E. Polygalov, I. Ermolina, G. Romanychev, Y. Zuev, and B. Milgotin. 1996. Time domain dielectric spectroscopy: An advanced measuring system. Rev. Sci. Instrum. 67:3208–3216.

Fellner-Feldegg, H. 1969. The measurement of dielectrics in the time domain. J. Phys. Chem. 73:616–623.

Feng, W., C.P. Lin, R.J. Deschamps, and V.P. Drnevich. 1999. Theoret-

ical model of a multisection time domain reflectometry measurement system. Water Resour. Res. 35:2321–2331.

Ferre, P.A., J.H. Knight, D.L. Rudolph, and R.G. Kachanoski. 1998. The sample areas of conventional and alternative time domain reflectometry probes. Water Resour. Res. 34:2971–2979.

Ferre, P.A., J.H. Knight, D.L. Rudolph, and R.G. Kachanoski. 2000. A numerically based analysis of the sensitivity of conventional and alternative time domain reflectometry probes. Water Resour. Res. 36:2461–2468.

Ferre, P.A., H.H. Nissen, P. Moldrup, and J.H. Knight. 2001. The sample area of time domain reflectometry probes in proximity to sharp dielectric permittivity boundaries, p. 195–209. In C.H. Dowding (ed.) Proc. Int. Symp. and Workshop on Time Domain Reflectometry for Innovative Geotechnical Applications, 2nd. Available at http://www.iti.northwestern.edu/tdr/tdr2001/proceedings/Final/TDR2001.pdf (verified 4 Sept. 2004). Infrastructure Technology Institute, Northwestern University, Evanston, IL.

Ferre, P.A., D.L. Rudolph, and R.G. Kachanoski. 1996. Spatial averaging of water content by time domain reflectometry: Implications for twin rod probes with and without dielectric coatings. Water Resour. Res. 32:271–279.

Ferre, P.A., D.L. Rudolph, and R.G. Kachanoski. 2003. The electrical conductivity response of a profiling time-domain reflectometry probe. Soil Sci. Soc. Am. J. 67:494–496.

Feynman, R.P., R.B. Leighton, and M. Sands. 1964. The Feynman lectures on physics. Vol. II. Addison-Wesley Publishing, Reading, MA.

Friedman, S.P. 1997. Statistical mixing model for the apparent dielectric constant of unsaturated porous media. Soil Sci. Soc. Am. J. 61:742–745.

Friedman, S.P. 1998. A saturation degree-dependent composite spheres model for describing the effective dielectric constant of unsaturated porous media. Water Resour. Res. 34:2949–2961.

Friedman, S.P., and S.B. Jones. 2001. Measurement and approximate critical path analysis of the pore-scale-induced anisotropy factor of an unsaturated porous medium. Water Resour. Res. 37:2929–2942.

Friel, R., and D. Or. 1999. Frequency analysis of time-domain reflectometry (TDR) with application to dielectric spectroscopy of soil constituents. Geophysics 64:1–12.

Gardner, C.M.K., T.J. Dean, and J.D. Cooper. 1998. Soil water content measurement with a high frequency capacitance sensor. J. Agric. Eng. Res. 71:395–403.

Gardner, C.M.K., D.A. Robinson, K. Blyth, and J.D. Cooper. 2001. Soil water content measurement. p. 1–64. In K. Smith and C. Mullins (ed.) Soil and environmental analysis: Physical methods. 2nd ed. Marcell Dekker, New York.

Gaskin, G.J., and J.D. Miller. 1996. Measurement of soil water content using a simplified impedance measuring technique. J. Agric. Eng. Res. 63:153–159.

Giese, K., and R. Tiemann. 1975. Determination of the complex permittivity from a thin sample time-domain reflectometry, improved analysis of the step response waveform. Adv. Molec. Relax. Processes 7:45–59.

Greacen, E.L. 1981. Soil water assessment by the neutron method. CSIRO, East Melbourne, Australia.

Gregory, P.J., P. Roland, J. Eastham, and S. Micin. 1995. Use of time domain reflectometry (TDR) to measure the water content of sandy soils. Aust. J. Soil Res. 33:265–276.

Hasted, J.B. 1973. Aqueous dielectrics. Chapman and Hall Ltd., London.

Hasted, J.B., D.M. Ritson, and C.H. Collie. 1948. Dielectric properties of aqueous solutions. Part I. J. Chem. Phys. 16:1–11.

Heimovaara, T.J. 1993. Design of triple wire time domain reflectometry probes in practice and theory. Soil Sci. Soc. Am. J. 57:1410–1417.

Heimovaara, T.J. 1994. Frequency domain analysis of time domain reflectometry waveforms. 1. Measurement of the complex dielectric permittivity of soils. Water Resour. Res. 30:189–199.

Heimovaara, T.J. 2001. Frequency domain modeling of TDR waveforms in order to obtain frequency-dependent dielectric properties of soil samples: A theoretical approach. Proc. Int. Symp. and Workshop on Time Domain Reflectometry for Innovative Geotechnical Applications, 2nd. Available at http://www.iti.northwestern.edu/tdr/tdr2001/proceedings/Final/TDR2001.pdf (verified 4 Sept. 2003).

Infrastructure Technology Inst., Northwestern University, Evanston, IL.

Heimovaara, T.J., and W. Bouten. 1990. A computer-controlled 36-channel time domain reflectometry system for monitoring soil water contents. Water Resour. Res. 26:2311–2316.

Heimovaara, T.J., W. Bouten, and J.M. Verstraten. 1994. Frequency domain analysis of time domain reflectometry waveforms. 2. A four component complex dielectric mixing model for soils. Water Resour. Res. 30:201–209.

Heimovaara, T.J., and E. de Water. 1993. A computer controlled TDR system for measuring water content and bulk electrical conductivity of soils. Rep. 41. Laboratory of Physical Geography and Soil Science, University of Amsterdam.

Heimovaara, T.J., E.J.G. de Winter, W.K.P. van Loon, and D.C. Esveld. 1996. Frequency dependent dielectric permittivity from 0 to 1 GHz: Time domain reflectometry measurements compared with frequency domain network analyzer measurements. Water Resour. Res. 32:3603–3610.

Herkelrath, W.N., S.P. Hamburg, and F. Murphy. 1991. Automatic, real-time monitoring of soil moisture in a remote field area with time domain reflectometry. Water Resour. Res. 27:857–864.

Hilhorst, M.A. 1998. Dielectric characterisation of soil. Publ. 98-01. IMAG-DLO, Wageningen, The Netherlands.

Hilhorst, M.A., J. Balendonck, and F.W.H. Kampers. 1993. A broad-bandwidth mixed analog/digital integrated circuit for the measurement of complex impedances. IEEE J. Solid State Circuits. 28:764–768.

Hillel, D. 1991. Out of the earth: Civilization and the life of the soil. Maxwell Macmillan International, New York.

Hoekstra, P., and A. Delaney. 1974. Dielectric properties of soils at UHF and microwave frequencies. J. Geophys. Res. 79:1699–1708.

Hokett, S.L., J.B. Chapman, and S.D. Cloud. 1992. Time domain reflectometry response to lateral soil water content heterogeneity. Soil Sci. Soc. Am. J. 56:313–316.

Hook, W.R., and N.J. Livingston. 1995. Propagation velocity errors in time domain reflectometry measurements of soil water. Soil Sci. Soc. Am. J. 59:92–96.

Hook, W.R., N.J. Livingston, Z.J. Sun, and P.B. Hook. 1992. Remote diode shorting improves measurement of soil water by time domain reflectometry. Soil Sci. Soc. Am. J. 56:1384–1391.

Huisman, J.A., C. Sperl, W. Bouten, and J.M. Verstraten. 2001. Soil water content measurements at different scales: Accuracy of time domain reflectometry and ground-penetrating radar. J. Hydrol. (Amsterdam) 245:48–58.

Huisman J.A., A.H. Weerts, T.J. Heimovaara and W. Bouten. 2002. Comparison of travel time analysis and inverse modeling for soil water content determination with time domain reflectometry. Water Resour. Res. 38 DOI:10.1029/2001WR000259.

Ibbotson, L. 1999. The fundamentals of signal transmission. Arnold, London.

IMKO. 1996. IMKO, TRIME, product guide. IMKO GmbH, Ettlingen, Germany.

Inoue, Y., T. Watanabe and K. Kitamura. 2001. Prototype time-domain reflectometry probes for measurement of moisture content near the soil surface for applications to 'on the move' measurements. Agric. Water Manage. 50:41–52.

Jackson, T.J., J. Schmugge, and E.T. Engman. 1996. Remote sensing applications to hydrology: Soil moisture. Hydrol. Sci. J. 41:517–530.

Jacobsen, O.H., and P. Schjonning. 1993. A laboratory calibration of time domain reflectometry for soil water measurement including effects of bulk density and texture. J. Hydrol. (Amsterdam) 151:147–158.

Jacobsen, O.H., and P. Schjonning. 1995. Comparison of TDR calibration functions for soil water determination. TDR, Applications in soil science. Proc. TDR Symp. Rep. 11. Danish Institute for Plant and Soil Science, Foulum, Denmark.

Jones, S.B., and S.P. Friedman. 2000. Particle shape effects on the effective permittivity of anisotropic or isotropic media consisting of aligned or randomly oriented ellipsoidal particles. Water Resour. Res. 36:2821–2833.

Jones, S.B., and D. Or. 2001. Extending TDR measurement range in saline soils using frequency domain methods. Proc. Int. Symp. and Workshop on Time Domain Reflectometry for Innovative Geotechnical Applications, 2nd. Available at http://www.iti.northwestern. edu/tdr/tdr2001/proceedings/Final/TDR2001.pdf (verified 4 Sept. 2003). Infrastructure Technology Inst., Northwestern University, Evanston, IL.

Jones, S.B., and D. Or. 2002. Surface area, geometrical and configurational effects on permittivity of porous media. J. Non-Cryst. Solids. 305:247–254.

Keller, G.V. 1989. Electrical properties. Section V *In* R.S. Carmichael (ed.) CRC practical handbook of physical properties of rocks and minerals. CRC Press, Boca Raton, FL.

Kelly, S.F., J.S. Selker, and L.L. Green. 1995. Using short soil moisture probes with high-bandwidth time domain reflectometry instruments. Soil Sci. Soc. Am. J. 59:97–102.

Kirkby, D. 1996. Finding the characteristics of arbitrary transmission lines. Amateur Radio Journal QEX December, p. 3–10.

Kluitenberg, G.J., and J.R. Philip. 1999. dual thermal probes near plane interfaces. Soil Sci. Soc. Am. J. 63:1585–1591.

Knight, J.H. 1991. Discussion of 'the spatial sensitivity of time-domain reflectometry' by J.M. Baker and R.J. Lascano. Soil Sci. 151:254–255.

Knight, J.H. 1992. Sensitivity of time domain reflectometry measurements to lateral variations in soil water content. Water Resour. Res. 28:2345–2352.

Knight, J.H. 1994. Sampling volume of TDR probes used for water content monitoring: Theoretical investigation. TDR Applications in Soil Science. Danish Institute for Plant and Soil Science, Foulum, Denmark.

Knight, J.H., P.A. Ferre, D.L. Rudolph, and R.G. Kachanoski. 1997. A numerical analysis of the effects of coatings and gaps upon relative dielectric permittivity measurement with time domain reflectometry. Water Resour. Res. 33:1455–1460.

Kraus J.D. 1984. Electromagnetics. 3rd ed. McGraw Hill, London.

Lathi, B.P. 1992. Linear signal and system analysis. Cambridge Press, Berkley.

Lide, D.R. 1992. Handbook of chemistry and physics. 73rd ed. CRC Press, Boca Raton, FL.

Lin, C.-P. 2003a. Analysis of nonuniform and dispersive time domain reflectometry measurement systems with application to the dielectric spectroscopy of soils. Water Resour. Res. 39 DOI:10.1029/2002 WR001418.

Lin, C.-P. 2003b. Frequency domain versus travel time analysis of TDR waveforms for soil moisture measurements. Soil Sci. Soc. Am. J. 67:720–729.

Long, D.S., J.M. Wraith, and G. Kegel. 2002. A heavy-duty time domain reflectometry soil moisture probe for use in intensive field sampling. Soil Sci. Soc. Am. J. 66:396–401.

Logsdon, S.D. 2000. Effect of cable length on time domain reflectometry calibration for high surface area soils. Soil Sci. Soc. Am. J. 64:54–61.

Lorrain, P., D.R. Corson, and F. Lorrain. 1988. Electromagnetic fields and waves. W.H. Freeman and Co., New York.

Maheshwarla, S.V., R. Venkatasubramanian, and R.F. Boehm. 1996. Comparison of time domain reflectometry performance factors for several dielectric geometri: Theory and experiments. Water Resour. Res. 31:1927–1933.

Malicki, M.A., R. Plagge, and C.H. Roth. 1996. Improving the calibration of dielectric TDR soil moisture determination taking into account the solid soil. Eur. J. Soil Sci. 47:357–366.

Maxwell, J.C. 1891. A treatise on electricity and magnetism. 1954 ed. Dover Publications Inc., New York.

Maxwell-Garnett, J.C. 1904. Colours in metal glasses and in metallic films. Philos. Trans. R. Soc., London A. 203:385–420.

Mojid, M.A., and H. Cho. 2002. Response of the core and shield rods of time-domain reflectometry probe to transverse soil-water content heterogeneity. J. Hydrol. (Amsterdam) 262:21–27.

Mojid, M.A., G.C.L. Wyseure, and D.A. Rose. 1997. Extension of the measurement range of electrical conductivity by time-domain reflectometry (TDR). Hydrol. Earth Syst. Sci. 1:175–183.

Nadler A., S. Dasberg, and I. Lapid. 1991. Time domain reflectometry measurements of water content and electrical conductivity of layered soil columns. Soil Sci. Soc. Am. J. 55:938–943.

Nadler, A., S.R. Green, I. Vogeler, and B.E. Clothier. 2002. Horizontal and vertical TDR measurements of soil water content and electrical conductivity. Soil Sci. Soc. Am. J. 66:735–743.

Nelson, S.O., L.H. Doderholm, and F.D. Yung. 1953. Determining the dielectric properties of grain. Agric. Eng. 34:608–610.

Nichol, C., R. Beckie, and L. Smith. 2002. Evaluation of uncoated and coated time domain reflectometry probes for high electrical conductivity systems. Soil Sci. Soc. Am. J. 66:1454–1465.

Nissen, H.H., P.A. Ferre, and P. Moldrup. 2003. Time domain reflectometry developments in soil science: I. unbalanced two-rod probe spatial sensitivity and sampling volume. Soil Sci. 168:77–83.

Nissen, H.H., P. Moldrup, T. Olesen, and P. Raskmark. 1999. Printed circuit board time domain reflectometry probe: Measurements of soil water content. Soil Sci. 164:454–466.

Noborio, K. 2001. Measurement of soil water content and electrical conductivity by time domain reflectometry: A review. Comput. Electron. Agric. 31:213–237.

Noborio, K., R. Horton, and C.S. Tan. 1999. Time domain reflectometry probe for simultaneous measurement of soil matric potential and water content. Soil Sci. Soc. Am. J. 63:1500–1505.

Noborio, K., K.J. McInnes, and J.L. Heilman. 1996. Measurements of soil water content, heat capacity and thermal conductivity with a single TDR probe. Soil Sci. 161:22–28.

Ochsner, T.E., R. Horton, and T. Ren. 2001. Simultaneous water content, air filled porosity and bulk density measurements with thermo-time domain reflectometry. Soil Sci. Soc. Am. J. 65:1618–1622.

Or, D., T. Hartwell, B. Fisher, R.A. Hubscher, and J.M. Wraith. 1998. WinTDR99—Users Guide (Windows-based time domain reflectometry program for measurement of soil water content and electrical conductivity). Available at http://soilphysics.usu.edu/wintdr/english/doc.html (accessed 11 July 2003, verified 9 Sept. 2003). Utah Agric. Exp. Stn. Res., Logan, UT.

Or, D., and V.P. Rasmussen. 1999. Effective frequency of TDR travel time-based measurement of bulk dielectric permittivity. Third Workshop on Electromagnetic Wave Interaction with Water and Moist Substances, Athens, GA. 12–13 Apr. 1999.

Or, D., and J.M. Wraith. 1999a. A new matric potential sensor based on time domain reflectometry. Water Resour. Res. 35:3399–3407.

Or, D., and J.M. Wraith. 1999b. Temperature effects on soil bulk dielectric permittivity measured by time domain reflectometry: A physical model. Water Resour. Res. 35:371–383.

Or, D., and J.M. Wraith. 2002. Soil water content and water potential relationships. p. 49–84. In A.W. Warrick (ed.) Soil physics companion. CRC Press, Boca Raton, FL.

Paltineanu, I.C., and J.L. Starr. 1997. Real-time water dynamics using multisensor capacitance probes: Laboratory calibration. Soil Sci. Soc. Am. J. 61:1576–1585.

Paquet, J.M., J. Caron, and O. Banton. 1993. In situ determination of the water desorption characteristics of peat substrates. Can. J. Soil Sci. 73:329–339.

Pepin, S., A.P. Plamondon, and J. Stein. 1992. Peat water content measurement using time domain reflectometry. Can. J. For. Res. 22:534–540.

Peplinski, N.R., F.T. Ulaby, and M.C. Dobson. 1995. Dielectric properties of soils in the 0.3–1.3 GHz range. IEEE Trans. Geosci. Remote Sens. 33:803–807.

Persson, M., and J.M. Wraith. 2002. Shaft-mounted time domain reflectometry probe for water content and electrical conductivity measurements. Available at www.vadosezonejournal.org. Vadose Zone J. 1:316–319.

Petersen L.W., A.Thomsen, P. Moldrup, O.H. Jacobsen and D.E. Rolston. 1995. High-resolution time domain reflectometry: Sensitivity dependency on probe design. Soil Sci. 159:149–154.

Pettinelli, E., A. Cereti, A. Galli, and F. Bella. 2002. Time domain reflectometry: Calibration techniques for accurate measurement of the dielectric properties of various materials. Rev. Sci. Instrum. 73:3553–3562.

Redman, J.D., and S.M. DeRyck. 1994. Monitoring non aqueous phase liquids in the subsurface with multilevel time domain reflectometry probes. Paper presented at Symposium and Workshop on Time Domain Reflectometry in Environmental, Infrastructure and Mining Applications, Evanston, IL. Sept 7–8 1994. U.S. Bur. of Mines, Washington, DC.

Ren, T., G.J. Kluitenberg, and R. Horton. 2000. Determining soil water flux and pore water velocity by a heat pulse technique. Soil Sci. Soc. Am. J. 64:552–560.

Ren, T., K. Noborio, and R. Horton. 1999. Measuring soil water content, electrical conductivity and thermal properties with a thermo-time domain reflectometry probe. Soil Sci. Soc. Am. J. 63:450–457.

Ritson, D.M., and J.B. Hasted. 1948. Dielectric properties of aqueous solutions. Part II. J. Chem. Phys. 16:11–21.

Robinson, D.A., J.P. Bell, and C.H. Batchelor. 1994. The influence of iron minerals on the determination of soil water content using dielectric techniques. J. Hydrol. (Amsterdam) 161:169–180.

Robinson, D.A., C.M.K. Gardner, and J.D. Cooper. 1999. Measurement of relative permittivity in sandy soils using TDR, capacitance and theta probes: Comparison, including the effects of bulk soil electrical conductivity. J. Hydrol. (Amsterdam) 223:198–211.

Robinson, D.A., C.M.K. Gardner, J. Evans, J.D. Cooper, M.G. Hodnett, and J.P. Bell. 1998. The dielectric calibration of capacitance probes for soil hydrology using an oscillation frequency response model. Hydrol. Earth Syst. Sci. 2:83–92.

Robinson, D.A., and S.P. Friedman. 2000. Parallel plates compared to conventional rods as TDR waveguides for sensing soil moisture. Subsurface Sens. Technol. Appl. 1:497–511.

Robinson, D.A., and S.P. Friedman. 2001. Effect of particle size distribution on the effective dielectric permittivity of saturated granular media. Water Resour. Res. 37:33–40.

Robinson, D.A., and S.P. Friedman. 2002. The effective permittivity of dense packing of glass beads, quartz sand and their mixtures immersed in different dielectric backgrounds. J. Non-Cryst. Solids 305:261–267.

Robinson D.A. and S.P. Friedman. 2003. A method for measuring the solid particle permittivity or electrical conductivity of rocks, sediments, and granular materials. J. Geophys. Res. B. 108, B2, 5:1–9.

Robinson, D.A., M. Schaap, S.B. Jones, S.P. Friedman, and C.M.K. Gardner. 2003. Considerations for improving the accuracy of permittivity measurement using TDR: Air/water calibration, effects of cable length. Soil Sci. Soc. Am. J. 67:62–70.

Roth, C.H., M.A. Malicki, and R. Plagge. 1992. Empirical evaluation of the relationship between soil dielectric constant and volumetric water content and the basis for calibrating soil moisture measurements by TDR. J. Soil Sci. 43:1–13.

Rothe, A., W. Weis, K. Kreutzer, D. Matthies, U. Hess, and B. Ansorge. 1997. Changes in soil structure caused by the installation of time domain reflectometry probes and their influence on the measurement of soil moisture. Water Resour. Res. 33:1585–1593.

Schaap, M., L. de Lange, and T.J. Heimovaara. 1996. TDR calibration of organic forest floor media. Soil Technol. 11:205–217.

Schaap, M., D.A. Robinson, S.P. Friedman, and A. Lazar. 2003. Measurement and modeling of the dielectric permittivity of layered granular media using time domain reflectometry. Soil Sci. Soc. Am. J. 67:1113–1121.

Selker, J.S., L. Graff, and T. Steenhuis. 1993. Nonivasive time domain reflectometry moisture measurement probe. Soil Sci. Soc. Am. J. 57:934–936.

Sen, P.N., C. Scala, and M.H. Cohen. 1981. A self-similar model for sedimentary rocks with application to the dielectric constant of fused glass beads. Geophysics 46:781–795.

Sharma, P.V. 1997. Environmental and engineering geophysics. Cambridge University Press, Cambridge, UK.

Sihvola, A. 1996. Dielectric mixture theories in permittivity prediction: Effect of water on macroscopic parameters. In A.W. Kraszewski (ed.) Microwave aquametry electromagnetic wave interaction with water-containing materials. IEEE Press, Piscataway, NJ.

Sihvola, A. 1999. Electromagnetic mixing formulas and applications. IEE Electromagnetic Waves Ser. 47. Inst. of Electrical Engineers, Stevenage, Herts, UK.

Sihvola, A., and J.A. Kong. 1988. Effective permittivity of dielectric mixtures. IEEE Trans. Geosci. Remote Sens. 26:420–429.

Simunek, J., and T. Vogel, and M.Th. van Genuchten. 1994. "SWMS-2D, Version 1.21." Res. Rep. 132. USDA-ARS, U.S. Salinity Laboratory, Riverside, CA.

Skaling W. 1992. TRASE: A product history. p. 187–207. In G.C. Topp (ed.) Advances in measurement of soil physical properties: Bringing theory into practice. SSSA Spec. Publ. 30. SSSA, Madison, WI.

Smith-Rose, R.L. 1933. The electrical properties of soil for alternating currents at radio frequencies. Proc. R. Soc. London. 140:359–377.

Smith-Rose, R.L. 1935. The electrical properties of soil at frequencies up to 100 megacycles per second; with a note on the resistivity of

ground in the United Kingdom. Proc. Phys. Soc. London 47: 923–931.

Spaans, E.J.A., and J.M. Baker. 1993. Simple baluns in parallel probes for time domain reflectometry. Soil Sci. Soc. Am. J. 57:668–673.

Stogryn, A. 1971. Equations for calculating the dielectric constant of saline water. IEEE Trans. Microwave Theory Technol. 19:733–736.

Strickland, J.A. 1970. Time-domain reflectometry measurements. Tektronix Inc., Beaverton, OR.

Sun, Z.J., G.D. Young, R.A. McFarlane, and B.M. Chambers. 2000. The effect of soil electrical conductivity on moisture determination using time-domain reflectometry in sandy soil. Can. J. Soil Sci. 80:13–22.

Thomas, A.M. 1966. In-situ measurement of moisture in soil and similar substances by 'fringe' capacitance. J. Sci. Instrum. 43:21–27.

Timlin, D., and Y. Pachepsky. 2002. Infiltration measurement using a vertical time-domain reflectometry probe and a reflection simulation model. Soil Sci. 167:1–8.

Topp, G.C., and J.L. Davis. 1985a. Time-domain reflectometry (TDR) and its application to irrigation scheduling. p. 107–127. *In* D. Hillel (ed.) Advances in irrigation. Vol. 3. Academic Press, London.

Topp, G.C., and J.L. Davis. 1985b. Measurement of soil water content using time-domain reflectometry (TDR): A field evaluation. Soil Sci. Soc. Am. J. 49:19–24.

Topp, G.C., J.L. Davis, and A.P. Annan. 1980. Electromagnetic determination of soil water content: Measurements in coaxial transmission lines. Water Resour. Res. 16:574–582.

Topp, G.C., J.L. Davis, and A.P. Annan. 1982a. Electromagnetic determination of soil water content using TDR: I. Applications to wetting fronts and steep gradients. Soil Sci. Soc. Am. J. 46:672–678.

Topp, G.C., J.L. Davis, and A.P. Annan. 1982b. Electromagnetic determination of soil water content using TDR: II. Evaluation of installation and configuration of parallel transmission lines. Soil Sci. Soc. Am. J. 46:678–684.

Topp, G.C., and W.D. Reynolds. 1998. Time domain reflectometry: A seminal technique for measuring mass and energy in soil. Soil Tillage Res. 47:125–132.

Topp, G.C., G. St-Amour, and B.A. Compton. 1996. Measuring cone resistance and water content with a TDR-penetrometer combination. p. 25–33. *In* J. Caron et al. (ed.) Proc. Eastern Canada Soil Structure Workshop, Merrickville, ON, Canada. Vol. 3. 21–22 Aug.

Topp, G.C., M. Yanuka, W.D. Zebchuk, and S.J. Zegelin. 1988. Determination of electrical conductivity using time domain reflectometry: Soil and water experiments in coaxial lines. Water Resour. Res. 24:945–952.

Topp, G.C., S. Zegelin, and I. White. 2000. Impact of real and imaginary components of relative permittivity on time domain reflectometry measurements in soils. Soil Sci. Soc. Am. J. 64:1244–1252.

van Gemert, M.J.C. 1973. High-frequency time-domain methods in dielectric spectroscopy. Philips Res. Rep. 28:530–572.

Vaz, C.M.P., L.H. Bassoi, and J.W. Hopmans. 2001. Contribution of water content and bulk density to field soil penetration resistance as measured by a combined cone penetrometer–TDR probe. Soil Tillage Res. 60:35–42.

Vaz, C.M.P., and J.W. Hopmans. 2001. Simultaneous measurement of soil penetration resistance and water content with a combined penetrometer–TDR moisture probe. Soil Sci. Soc. Am. J. 65:4–12.

Vaz, C.M.P., J.W. Hopmans, A. Macedo, L.H. Bassoi, and D. Wildenschilde. 2002. Soil water retention measurements using a combined tensiometer–coiled time domain reflectometry probe. Soil Sci. Soc. Am. J. 66:1752–1759.

von Hippel, A.R. (ed.) 1954. Dielectrics materials and applications. MIT Press, Cambridge, MA.

Weerts, A.H., J.A. Huisman, and W. Bouten. 2001. Information content of time domain reflectometry waveforms. Water Resour. Res. 37:1291–1299.

Weiler, K.W., T.S. Steenhuis, J. Boll, and K.-J.S. Kung. 1998. Comparison of ground penetrating radar and time domain reflectometry as soil water sensors. Soil Sci. Soc. Am. J. 62:1237–1239.

Whalley, W.R. 1993. Considerations on the use of time domain reflectometry (TDR) for measuring soil water content. J. Soil Sci. 44:1–9.

White, I., J.H. Knight, S.J. Zegelin, and G.C. Topp. 1994. Comments on "Considerations on the use of time domain reflectometry (TDR) for measuring soil water content." Eur. J. Soil Sci. 45:503–508.

White, I., and S.J. Zegelin. 1995. Electric and dielectric methods for monitoring soil-water content. p. 343–385. *In* L.G. Wilson et al. (ed.) Handbook of vadose zone characterization and monitoring. Lewis Publ., Boca Raton, FL.

Wobschall D. 1978. A frequency shift dielectric soil moisture sensor. IEEE Trans. Geosci. Electron. 16:112–118.

Wright, W.C., R.E. Yoder, N.R. Rainwater, and E.C. Drumm. 2001. Calibration of five-segmented time domain reflectometry probes for water content measurement in high density materials. Geotech. Test. J. 24(2):172–184.

Yanuka, M., G.C. Topp, S. Zegelin, and W.D. Zebchuk. 1988. Multiple reflection and attenuation of time domain reflectometry pulses: Theoretical considerations for applications to soil and water. Water Resour. Res. 24:939–944.

Young, G.D., B.A. Adams, and G.C. Topp. 2000. A portable data collection system for simultaneous cone penetrometer force and volumetric soil water content measurements. Can. J. Soil Sci. 80: 23–31.

Zegelin, S.J., I. White, and D.R. Jenkins. 1989. Improved field probes for soil water content and electrical conductivity measurement using time domain reflectometry. Water Resour. Res. 25:2367–2376.